Doctoral Dissertation

博士論文

Analysis of roles of AMPK in neuronal migration of developing neocortex

(発生期大脳新皮質の神経細胞移動における AMPK の機能解析)

A Dissertation Submitted for the Degree of Doctor of Philosophy
submitted on January 2020

令和 2 年 1 月博士（理学）申請

Department of Biophysics and Biochemistry,
Graduate School of Science, The University of Tokyo

東京大学大学院理学系研究科生物化学専攻

Yasuki Naito

内藤　泰樹

Abstract

The microtubule motor cytoplasmic dynein contributes to radial migration of newborn pyramidal neurons in the developing neocortex. Here I show that AMP-activated protein kinase (AMPK) mediates the nucleus-centrosome coupling, a key process for radial neuronal migration that relies on dynein. Depletion of the catalytic subunit of AMPK in migrating neurons impairs this coupling as well as neuronal migration. AMPK shows overlapping cellular distribution with cytoplasmic dynein and the two proteins interact with each other. Pharmacological inhibition or activation of AMPK modifies the phosphorylation states of dynein intermediate chain (DIC) and dynein functions. Further, AMPK phosphorylates DIC at Ser81. Expression of a phospho-resistant mutant of DIC retards neuronal migration in a similar way to AMPK depletion. Conversely, expression of the phospho-mimetic mutant of DIC alleviates impaired neuronal migration caused by AMPK depletion. Thus, AMPK-regulated dynein function via Ser81 phosphorylation is critical for radial neuronal migration.

Contents

1. Introduction

Neuronal migration is a fundamental process for proper brain development. Defects in this process cause severe neurodevelopmental disorders (Feng and Walsh, 2001; Guerrini and Parrini, 2010; Kato and Dobyns, 2003; Reiner et al., 2016). In the developing cerebral cortex, postmitotic neurons migrate long distance along fibers of radial glial cells from their birthplace in the ventricular zone (VZ) toward the pial surface (Hatten, 1999; Kriegstein and Noctor, 2004; Marín et al., 2010) (Fig. 1). As cortical neurons migrate, they show bipolar morphology with a long, thick leading process oriented toward the pia and a thin tailing process directing to the ventricle. To undergo neuronal migration, cortical neurons direct a series of highly-organized subcellular events including extension of the leading process and forward movement of the centrosome ahead of the nucleus. These changes are followed by translocation of the nucleus toward the centrosome (Bertipaglia et al., 2018; Cooper, 2013; Tsai and Gleeson, 2005). The nuclear translocation following the centrosomal forward movement is key for neuronal migration, and these events rely on proper modulation of the microtubule/actin cytoskeletons and their motor proteins (Fig. 2). In migrating neurons, the microtubule network emanating from the centrosome extends out in the leading process and reward to surround the nucleus (Bertipaglia et al., 2018; Cooper, 2013; Tsai and Gleeson, 2005) . Cytoplasmic dynein, a minus end-directed motor of microtubules, is enriched at the nuclear envelope and in the dilated region (known as cytoplasmic swelling) near the base of the leading process (Tsai et al., 2007; Zhang et al., 2009). It has been proposed that this regional (compartmentalized) localization of dynein is required for pulling the centrosome/nucleus forward along the microtubules. In fact, knockdown of dynein heavy chain or dynein-associated proteins such as Lis1 (also

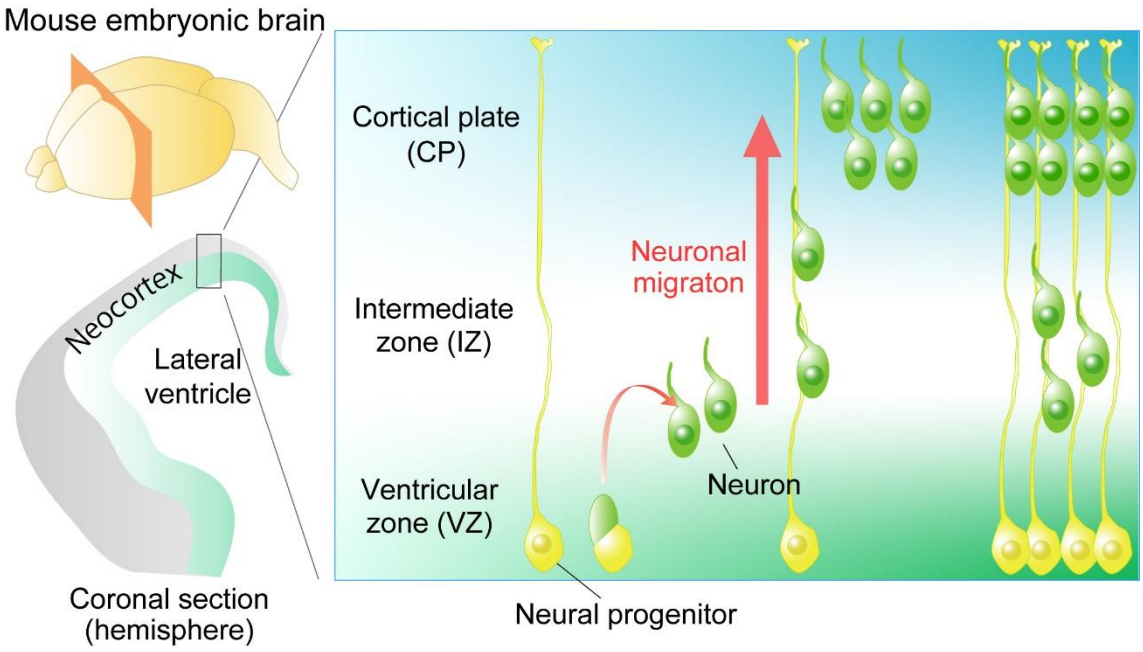

Fig. 1 Schematic diagram of neurogenesis and neuronal migration in the developing neocortex.

Neurons (green) are born from neural progenitor cells (radial glial cells, yellow) located in the ventricular zone (VZ). Newborn neurons migrate toward the pial surface through the intermediate zone (IZ) of the neocortex along the fiber of neural progenitor cells and form the cortical plate (CP).

known as Pafah1b1) and Ndel1/Nde1 weakens the coordination between the centrosome and the nucleus, and inhibits the centrosomal/nuclear forward movement (Shu et al., 2004; Tanaka et al., 2004). In addition to the microtubules and dynein, the actin cytoskeleton and myosin contribute to nuclear translocation in migrating neurons. It is supposed that, when positioned ahead of the nucleus, actomyosin pulls it (Solecki et al., 2009); when behind the nucleus, actomyosin squeezes the rear side of the cells to push the nucleus forward (Schaar and McConnell, 2005). In brief, motor proteins play a key role in nuclear migration but the signals that regulate their behaviors in migrating neurons remain poorly understood.

Previous studies have revealed that the Ser/Thr kinase LKB1 (Liver kinase B1, also known as Par-4 or STK11) plays an important role in both centrosomal forward movement and nuclear movement in migrating neurons (Asada and Sanada, 2010; Asada et al., 2007). Regarding the centrosomal movement, the authors have shown that LKB1 mediates phosphorylation and thereby inactivation of GSK3β at the leading process tip to pull the centrosome up within the leading process (Asada and Sanada, 2010). On the other hand, molecular mechanisms underlying the nuclear movement directed by LKB1 remains unknown. It is known that LKB1 is the master activator of 14 kinases (known as AMPK-related protein kinases), including AMPKαs, SAD/BRSK kinases (Synapses of amphid defective, Brain specific kinases), NUAKs (Nua kinases), SIKs (Salt-inducible kinases), and MARKs (Microtubule-affinity regulating kinases), MELK (Maternal embryonic leucine zipper kinase) (Jaleel et al., 2005; Lizcano et al., 2004). Therefore, it is possible that one of the downstream kinases of LKB1 plays roles in the regulation of the nuclear migration. In this study, I found that AMPK contributes to nuclear forward movement in migrating neurons.

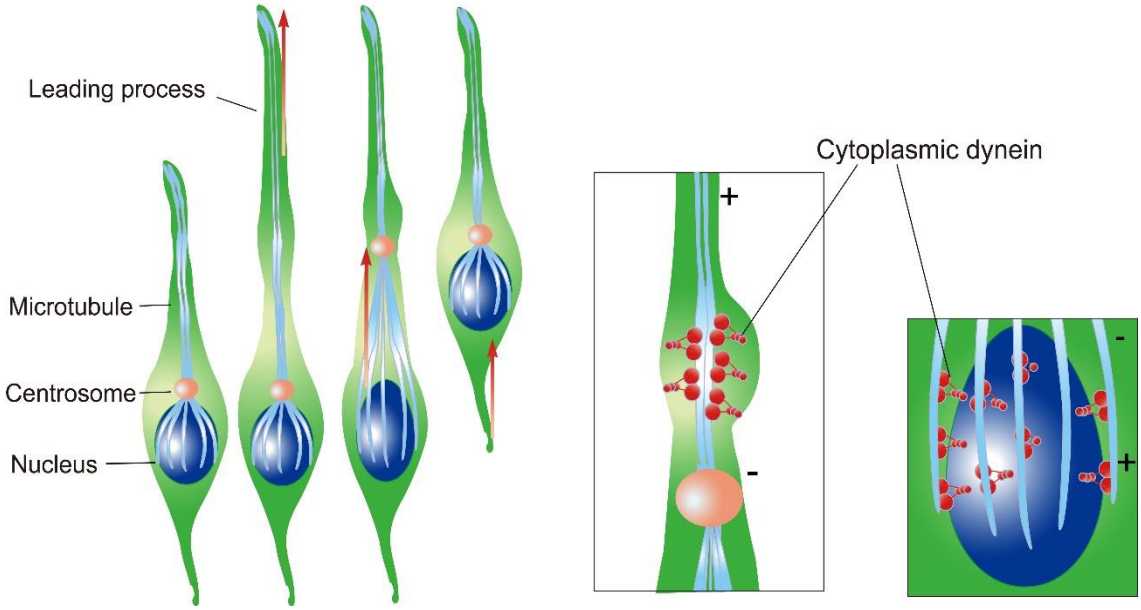

Fig. 2 Schematic diagram of neuronal migration in the developing neocortex. Migratory neurons have a thick process oriented in the direction of migration (leading process), and a trailing process. As neurons migrate, neurons undergo the cycle of extension of the leading process, forward movement of the centrosome, and nuclear migration towards the centrosome. In migratory neurons, the microtubule network emanated from the centrosome extends out in the leading process and reward to surround the nucleus, and cytoplasmic dynein, a microtubule motor, enriched at the swelling (within the leading process) and nuclear envelope is supposed to direct the centrosomal and nuclear movement, respectively.

AMPK consists of three subunits, a catalytic α-subunit, and regulatory β- and γ-subunits (Fig. 3). Full activation of AMPK requires its phosphorylation at Thr172 in the kinase domain of the α-subunit. In addition, AMP binding to the γ-subunit is known to promote net phosphorylation at Thr172 through protecting Thr172 from its dephosphorylation and enhancing the association of AMPK with the upstream kinase (Jeon, 2016; Stein et al., 2000). To date, two protein kinases, liver kinase B1 (LKB1) and calcium/calmodulin-dependent protein kinase kinase β (CaMKK β), have been identified as major upstream kinases responsible for the Thr172 phosphorylation and thus activation of AMPK in mammalian cells (Dasgupta and Chhipa, 2016; Jeon, 2016).

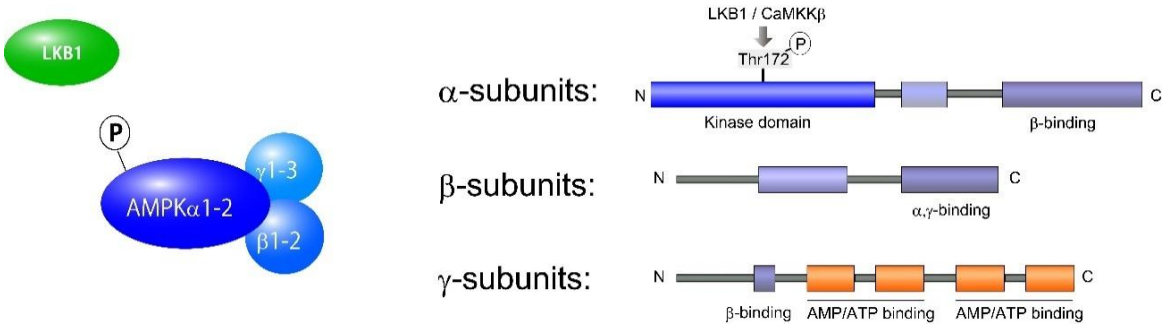

Fig. 3 Schematic diagram of AMPK subunits.

AMPK consists of three subunits: a catalytic α subunit, and regulatory β- and γ-subunits, and each subunit is coded by respective two, two, and three genes. AMPK is activated by phosphorylation of the Thr172 residue in the kinase domain of α-subunit, and this is mediated by upstream kinases such as LKB1 and CaMKKβ. AMP/ ATP binding sites are located at the γ-subunit.

In the present study, I demonstrated that AMPK regulates cytoplasmic dynein behavior and drives nuclear migration in migrating neurons of the developing neocortex. Knockdown of AMPKα causes defects in nuclear migration, thereby impeding neuronal migration. AMPK associates with dynein, phosphorylates dynein intermediate chain at Ser81, and modulates dynein functions. Furthermore, overexpression of the phospho-resistant mutant of dynein intermediate chain causes retardation of neuronal migration in a similar fashion to AMPK depletion. Conversely, impaired neuronal migration observed upon AMPK depletion is counterbalanced by co-expression of the phospho-mimetic mutant of dynein intermediate chain. Thus, AMPK modulates dynein behavior and nuclear migration in migratory neurons.

2. Results

2-1. Expression of AMPKα and Thr172-phosphorylated AMPKα in the developing neocortex

In mammals, the alpha catalytic subunit of AMPK (AMPKα) has two isoforms, AMPKα1 and AMPKα2. First, I examined the protein expression of the two isoforms in the developing neocortex. AMPKα1 and AMPKα2 were both expressed in the developing mouse neocortex from embryonic day (E) 13 to postnatal day (P) 0, as assessed by western blotting with antibodies specific to AMPKα1 and AMPKα2 (Fig. 4A). I also examined total AMPKα expression using an antibody that recognizes both AMPKα1 and AMPKα2 and found that total AMPKα levels were relatively constant during the examined period (E13 to P0) (Fig. 4A). Moreover, Thr172-phosphorylated / activated AMPKα (pAMPKα) that was detected with an antibody recognizing the Thr172-phosphorylated form of both AMPKα1 and AMPKα2, was also present in the developing neocortex throughout this period, with relatively low levels at E13 and higher levels at E15-P0.

Immunohistochemical analysis indicated that total AMPKα was expressed in the VZ as well as in the cortical plate (CP) and intermediate zone (IZ) where migrating neurons reside abundantly. Immunofluorescent signals of pAMPKα were observed in a punctate pattern in the VZ/IZ/CP and showed remarkable overlapping localization with a centrosomal marker, pericentrin, in these regions (Fig. 4B). Detailed analysis of migrating neurons transfected with GFP and the centrosomal marker DsRed-Centrin2 confirmed that pAMPKα was enriched around the centrosome (Fig. 4C).

I further investigated the subcellular distribution of pAMPKα in primary cortical

neurons and Cos-7 cells. In cultured cortical neurons, pAMPKα signals were prominent around the centrosome, and weak/diffuse signals were also present in the cytoplasm (Fig. 5A). In Cos-7 cells, pAMPKα and AMPKα signals were punctate and highly enriched in the proximal part of the interphase microtubule arrays emanating from the centrosome. At the centrosome and on the microtubule arrays, pAMPKα and AMPKα showed substantial overlapping distribution with dynein intermediate chain, a subunit of cytoplasmic dynein, and LIS1, a dynein-associated protein (Fig. 5A, B). Together, these observations suggest that AMPKα likely decorates microtubules in a similar fashion to cytoplasmic dynein.

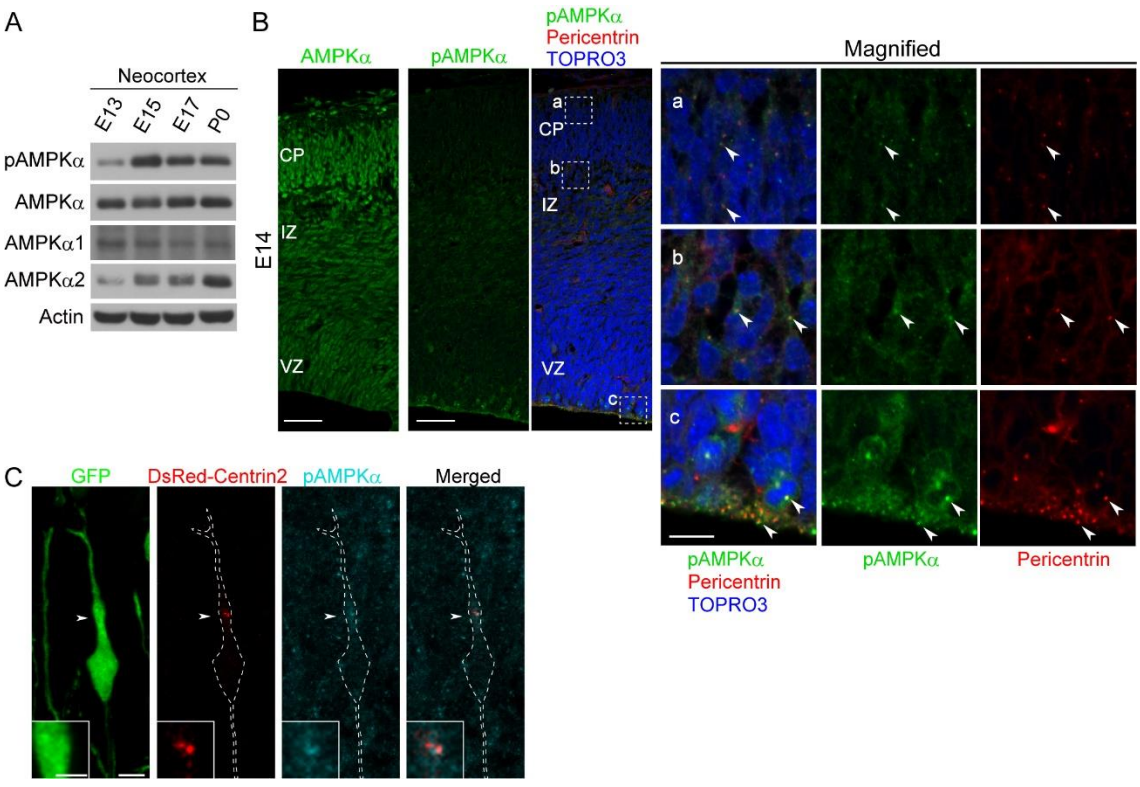

Fig. 4 Expression of AMPKα in the developing mouse neocortex.

(A) Lysates prepared from E13, E15, E17 and P0 neocortices were immunoblotted with antibodies indicated. **(B)** E14 neocortical sections immunostained with antibodies against AMPKα, pAMPKα, and Pericentrin. Images of the cerebral wall are shown (left panels). The boxed areas of the image are magnified and shown in right panels. TO-PRO-3 iodide staining shows Nuclei. Two examples of pAMPKα-positive puncta are indicated by arrowheads in each panel. Scale bars, 50 μm (left panels) and 10 μm (right panels). **(C)** Plasmids that express GFP and DsRed-Centrin2 were together electroporated into E14 mouse neocortex, and brains were fixed at E17. The brain sections were immunostained with antibodies against pAMPKα and GFP. High magnification images of a GFP-positive migratory neuron located at CP are shown. The GFP-positive neuron is outlined with a dashed line. Arrowheads indicate the position of the centrosome. Magnified images around the centrosome are shown as insets. Scale bars, 5 μm and 2 μm (insets).

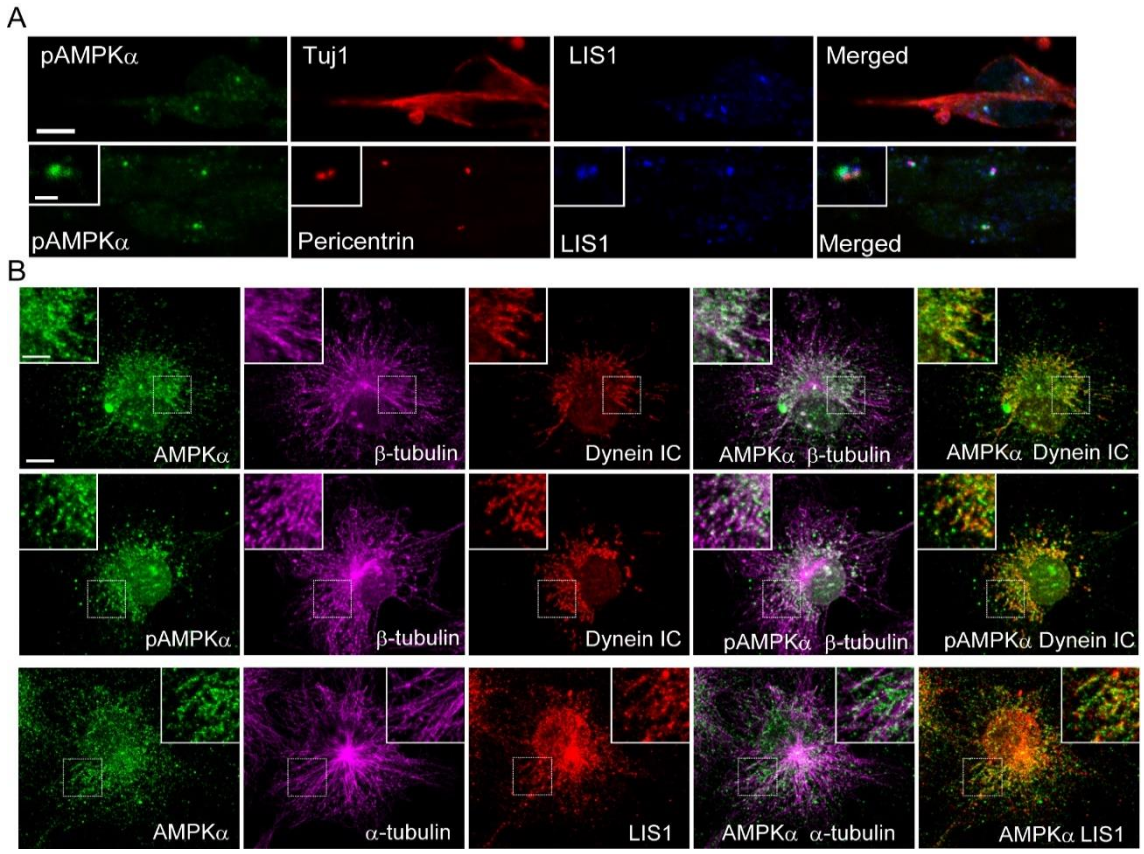

Fig. 5 Subcellular localization of AMPKα.

(A) Neocortical neurons at days in vitro 2 (DIV 2) were immunostained with antibodies against pAMPKα, Tuj1 (a neuronal marker), Pericentrin and LIS1. Magnified images around the centrosome are shown as insets. Scale bars, 5 μm and 1 μm (insets). **(B)** Cos-7 cells were immunostained with antibodies indicated. Scale bars, 10 μm and 5 μm (insets).

2-2. AMPKα depletion causes defects in neuronal migration

In order to examine the role of AMPK in neuronal migration in the developing neocortex, I investigated the effects of AMPKαs knockdown. For that, I generated plasmids expressing short hairpin RNAs against AMPKα1 (AMPKα1 shRNA and shRNA#2) and AMPKα2 (AMPKα2 shRNA and shRNA#2). The shRNA constructs effectively silenced the expression of the respective AMPKα that were transiently expressed in Cos-7 cells (Fig. 6A). On the other hand, expression of shRNA-resistant mutants of AMPKα1 (AMPKα1^{res}) and AMPKα2 (AMPKα2^{res}) that contain two silent mutations within the target sequence of the AMPKα1 shRNA and AMPKα2 shRNA were not affected by their respective shRNA constructs (Fig. 6A). In addition, endogenous AMPKα expression was remarkably diminished in AMPKα shRNA-introduced primary cortical neurons (Fig. 6B).

To determine whether AMPK is required for neuronal migration in the developing neocortex, I electroporated the AMPKα shRNA constructs into E14 mouse neocortices, together with the plasmid expressing GFP (Fig. 7). In neocortices electroporated with the control shRNA at E14, GFP-labeled control cells at E17 were mainly located at the IZ (28.3 ± 1.4%) and CP (67.0 ± 2.0%), and they migrate further into the CP at E18 (IZ: 5.6 ± 2.4%, CP: 92.3 ± 3.5%). In contrast, AMPKα2 shRNA-introduced cells were mainly located at IZ at E17 (86.7 ± 0.7%) and E18 (67.8 ± 1.0%) (Fig. 8A, B). Similar abnormal distribution pattern of GFP-labeled neurons was observed in neocortices electroporated with the AMPKα1 shRNA construct as well as with a mixture of the AMPKα1 shRNA plasmid and the AMPKα2 shRNA plasmid (hereafter referred to as AMPKα1/2 shRNA).

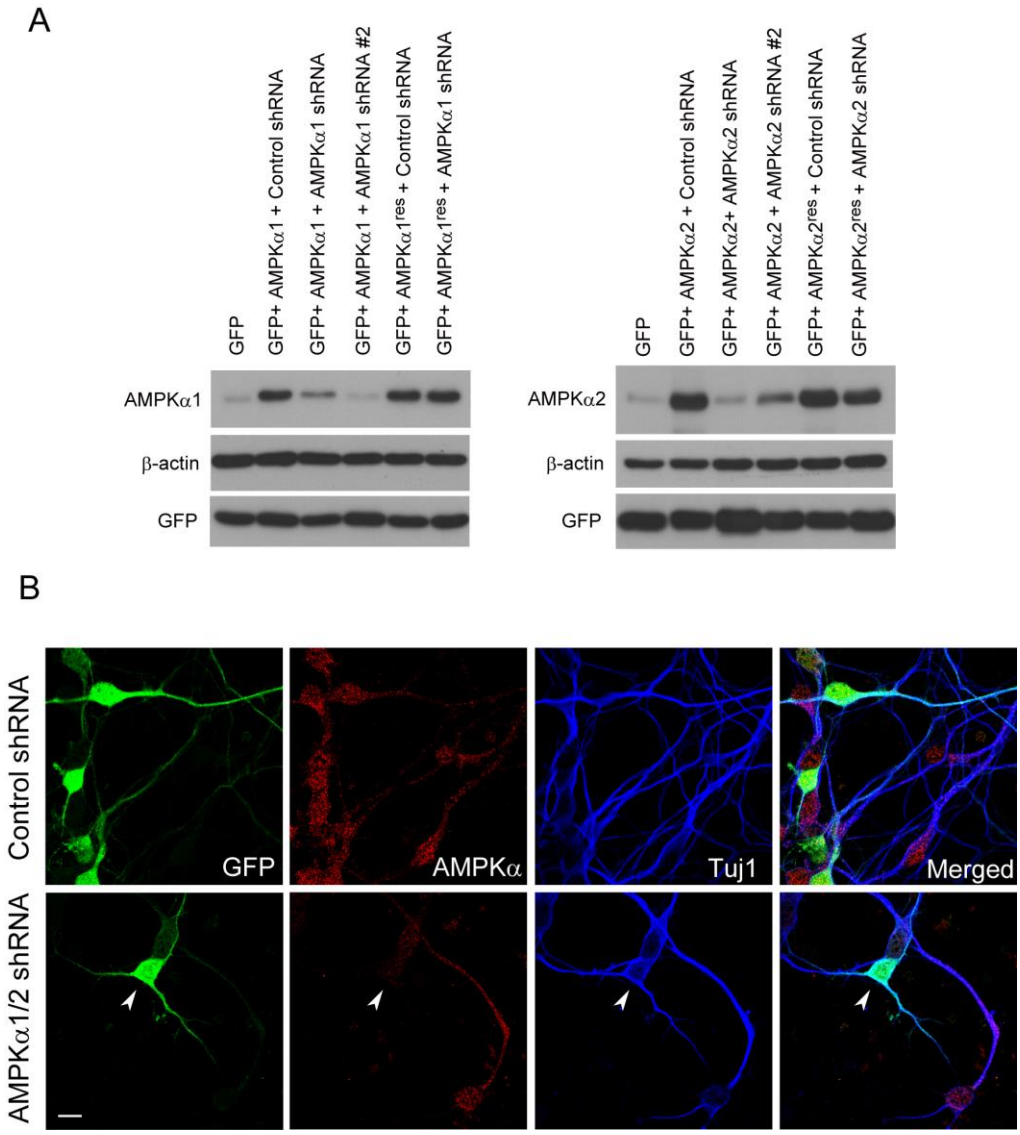

Fig. 6 Validation of AMPKα shRNA plasmids

(A) Cos-7 cells (right panels) were transiently transfected with constructs indicated. The cell lysates were prepared 48 hours after transfection. The cell lysates were subjected to immunoblotting with antibodies against AMPKα1, AMPKα2, β-actin and GFP. GFP serves as transfection control. **(B)** Dispersed neocortical cells were prepared from E14 brains, transfected with either the control shRNA plasmid or a mixture of the AMPKα1 shRNA plasmid and the AMPKα2 shRNA plasmid (AMPKα1/2 shRNA), together with construct that express GFP. DIV 4 cells were immunostained with antibodies against AMPKα, GFP and Tuj1. Representative images are shown. An arrowhead indicates an AMPKα shRNA-introduced neuron. Scale bar, 10 μm.

Furthermore, introduction of second shRNA plasmids for AMPKα1 (AMPKα1 shRNA#2) and for AMPKα2 (AMPKα2 shRNA#2) also significantly retarded neuronal migration (Fig. 9A). Of note, GFP-positive cells in the CP/IZ in the neocortices electroporated with the AMPKα shRNA plasmids display normal bipolar morphology, just like control neurons. In addition, mis-positioning of GFP-labeled cells in the neocortices electroporated with the AMPKα1 shRNA construct and the AMPKα2 shRNA construct was unlikely caused by neuronal apoptosis: Apoptosis detected with cleaved caspase 3 antibody was not enhanced upon electroporation of the AMPKα1/2 shRNA construct when compared to control shRNA (Fig. 10). Moreover, defects in neuronal positioning in AMPKα1 shRNA- and AMPKα2 shRNA-introduced neocortices were significantly rescued by co-expression of respective AMPKα1^{res} and AMPKα2^{res} that are resistant to RNAi (Figs. 8C, 8D, 9B). These results confirm the specificity of AMPKα shRNAs and indicate that impaired neuronal migration of AMPKα shRNA-introduced neurons was indeed caused by AMPKα depletion.

Furthermore, expression of kinase-dead AMPKα (T172A AMPKα and D157A AMPKα) (Stein et sal., 2000) did not rescue migration defects of AMPKα-depleted neurons (Figs. 8C, 8D, 9C), thereby suggesting that AMPKα kinase activity is required for proper migration of newborn cortical neurons. In addition, at P4, almost all AMPKα-depleted neurons were found within the CP (Fig. 11). Thus, AMPKα depletion strongly delays neuronal migration, rather than arresting it. Of note, AMPKα-depleted neurons at P4 resided in more superficial layers when compared with control neurons, probably due to their delayed migration (Fig. 11).

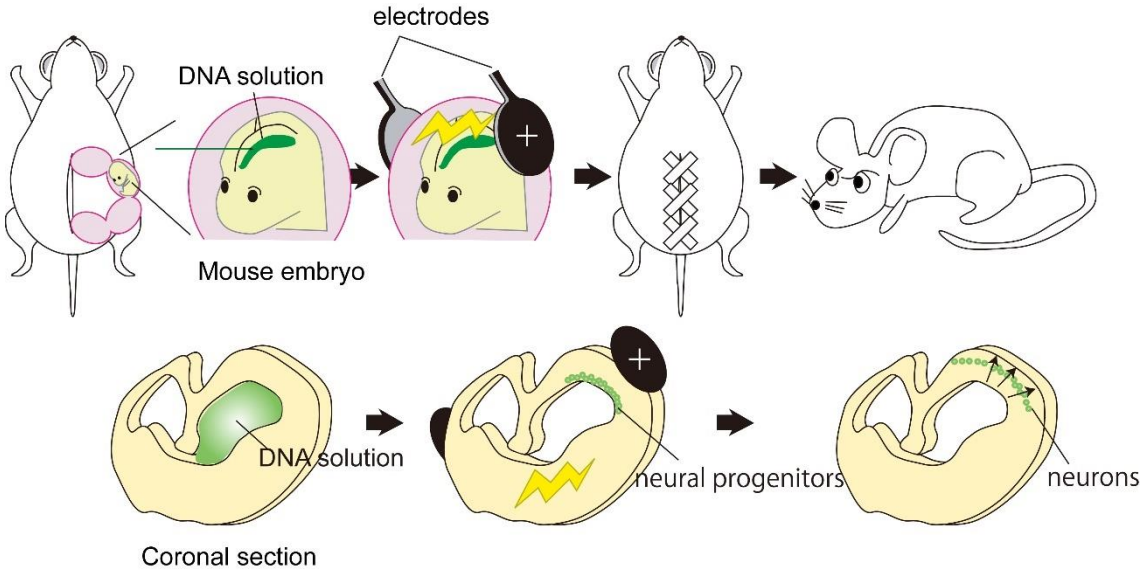

Fig. 7 *In utero* electroporation

Pregnant mice are anesthetized. DNA solutions are injected into lateral ventricle of the mouse embryos. Neural progenitors located at VZ are transfected with DNA upon electrical pulses applied. Neurons carrying DNA derived from neural progenitors are analyzed after a certain period of time.

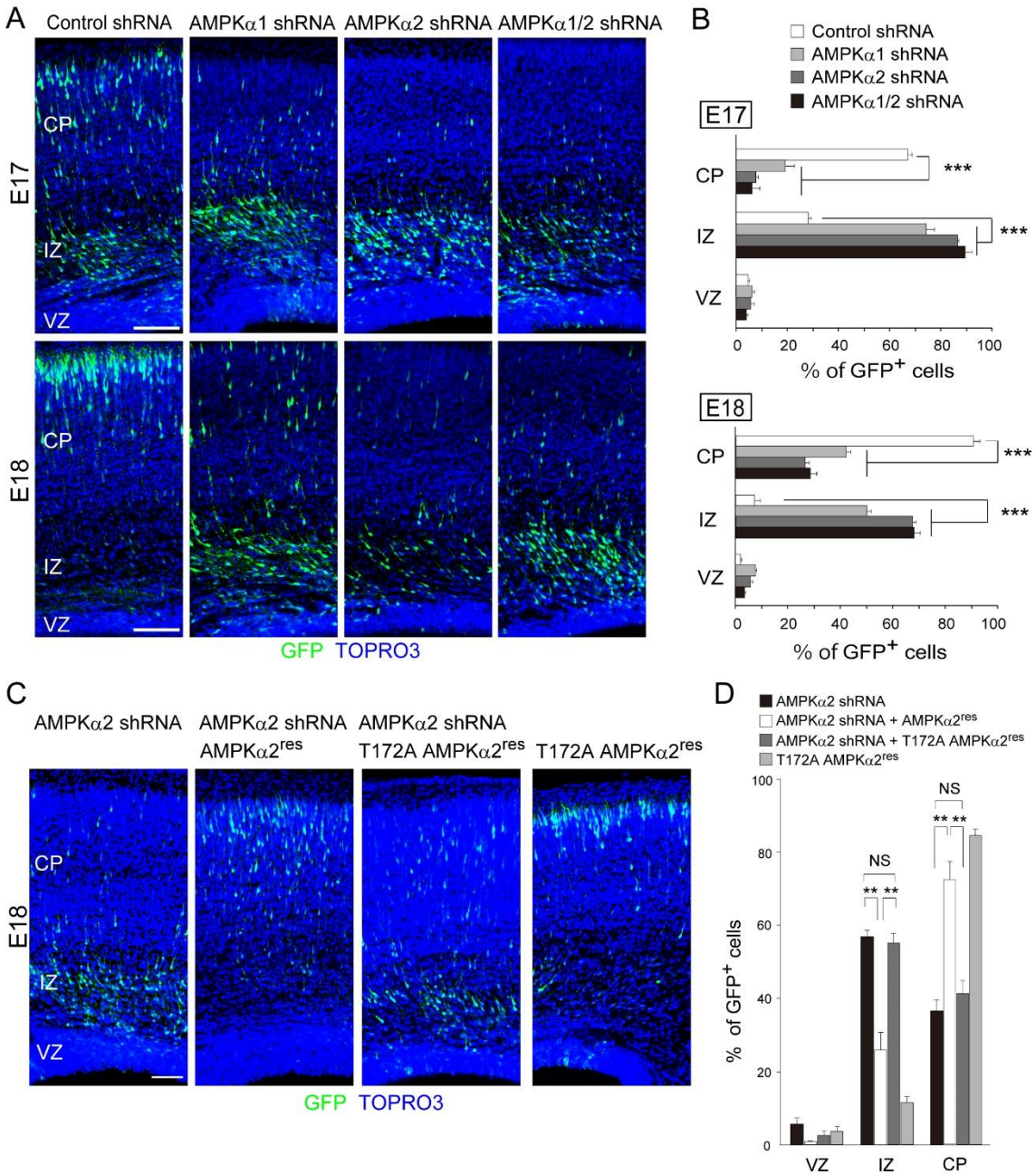
A
Control shRNA
AMPKα1 shRNA
AMPKα2 shRNA
AMPKα1/2 shRNA
E17
E18
CP
IZ
VZ
GFP TOPRO3
B
Control shRNA
AMPKα1 shRNA
AMPKα2 shRNA
AMPKα1/2 shRNA
E17
E18
CP
IZ
VZ
***
0 20 40 60 80 100
% of GFP+ cells
C
AMPKα2 shRNA
AMPKα2 shRNA AMPKα2res
AMPKα2 shRNA T172A AMPKα2res
T172A AMPKα2res
E18
CP
IZ
VZ
GFP TOPRO3
D
AMPKα2 shRNA
AMPKα2 shRNA + AMPKα2res
AMPKα2 shRNA + T172A AMPKα2res
T172A AMPKα2res
% of GFP+ cells
0 20 40 60 80 100
NS
** **
VZ
IZ
CP

Fig. 8 Knock-down of AMPKα impairs neuronal migration.

(A, B) Plasmids expressing control shRNA and AMPKα shRNAs as indicated were electroporated into E14 neocortices with the plasmid expressing GFP. Brains were fixed at E17 or E18, and brain sections were immunostained with an antibody against GFP. TO-PRO-3 iodide staining shows Nuclei. Representative images are shown in (A). The percentage of GFP-positive neurons in the CP, IZ, and VZ was measured and is plotted in (B) as the mean ± s.e.m. (n = 3-4 brains). ***p < 0.001 versus control by two-tailed Welch's *t* test. In (B), total 1662 (E17) and 1805 (E18) neurons were counted for control shRNA, 1423 (E17) and 1238 (E18) cells for AMPKα1 shRNA, 938 (E17) and 1467 (E18) cells for AMPKα2 shRNA, 801 (E17) and 1944 (E18) cells for AMPKα1/2 shRNA. **(C, D)** Plasmids expressing AMPKα2 shRNA, AMPKα2^{res} (AMPKα2 resistant to AMPKα2 shRNA) and a kinase-dead form (T172A) of AMPKα2^{res} (AMPKα2 resistant to AMPKα2 shRNA) as indicated were electroporated into E14 neocortices with the plasmid expressing GFP. E18 brain slices were immunostained with an antibody against GFP. Representative images are shown in (C). The percentage of GFP-positive cells in the CP, IZ, and VZ was measured and is plotted in (D) as the mean ± s.e.m. (n = 4-5 brains). **p < 0.01 by two-tailed Welch's *t* test. NS, not significant. In (D), total 518 cells were counted for AMPKα2 shRNA, 857 cells for AMPKα2 shRNA + AMPKα2^{res}, 851 cells for AMPKα2 shRNA + T172A AMPKα2^{res}, 675 cells for T172A AMPKα2^{res}. Scale bars, 100 μm.

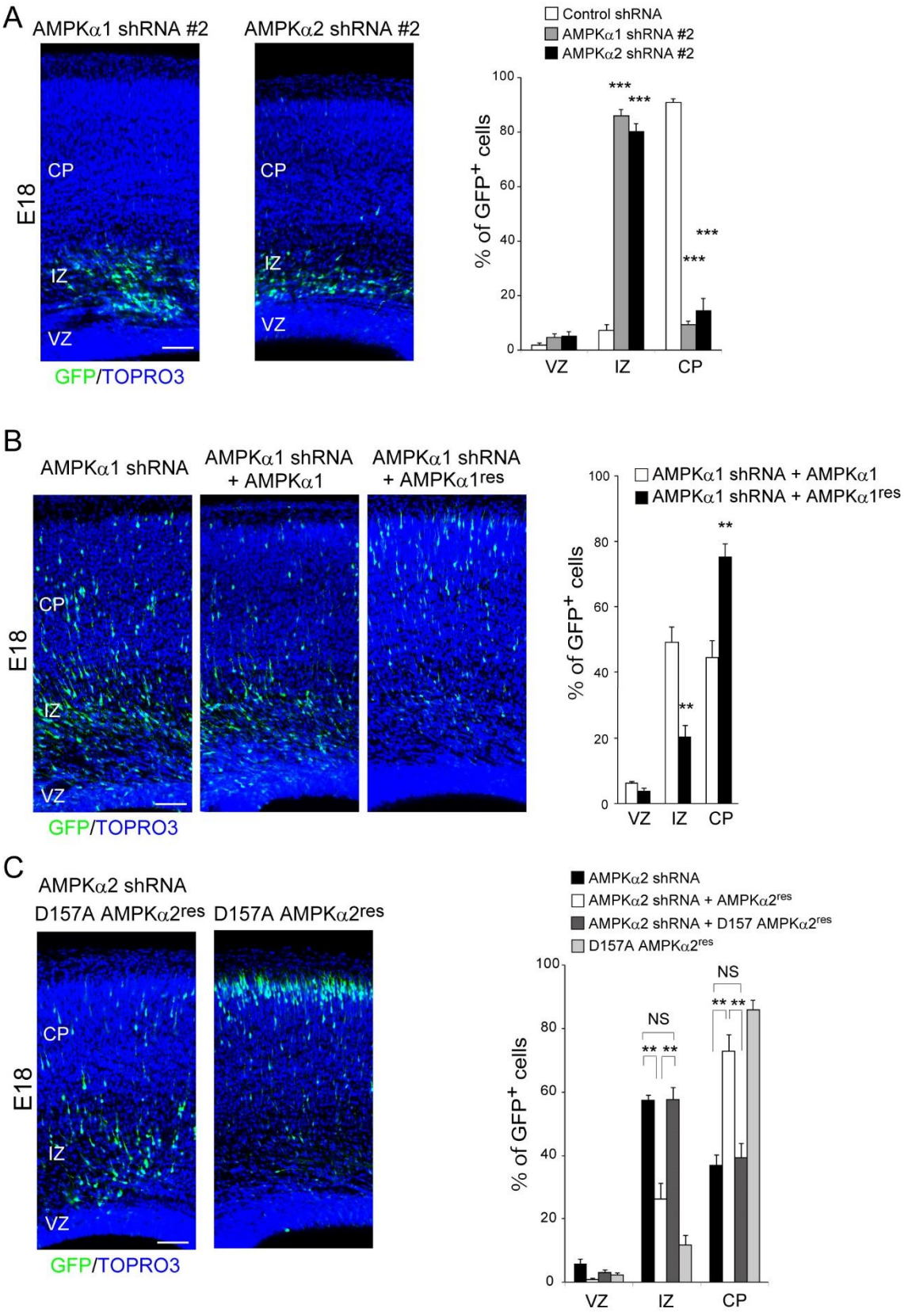
A
AMPKα1 shRNA #2
AMPKα2 shRNA #2
E18
CP
IZ
VZ
GFP/TOPRO3
Control shRNA
AMPKα1 shRNA #2
AMPKα2 shRNA #2
% of GFP+ cells
VZ
IZ
CP
B
AMPKα1 shRNA
AMPKα1 shRNA + AMPKα1
AMPKα1 shRNA + AMPKα1res
AMPKα1 shRNA + AMPKα1
AMPKα1 shRNA + AMPKα1res
C
AMPKα2 shRNA
D157A AMPKα2res
AMPKα2 shRNA + AMPKα2res
AMPKα2 shRNA + D157 AMPKα2res
NS

Fig. 9 Effects of AMPKα-depletion on neuronal migration

(A) Either the AMPKα1 shRNA#2 plasmid or the AMPKα2 shRNA#2 plasmid was electroporated into E14 neocortices with the plasmid that express GFP. E18 brain slices were immunostained with anti-GFP antibody. TO-PRO-3 iodide staining shows Nuclei. The percentage of GFP-positive neurons in the CP, IZ, and VZ was measured and is plotted as the mean ± s.e.m. (n = 4 embryos, more than 1300 neurons were analyzed in each condition). ***p < 0.001 versus control by two-tailed Welch's *t* test. **(B)** Plasmids expressing AMPKα1 shRNA, AMPKα1, and AMPKα1^{res} (AMPKα1 resistant to AMPKα1 shRNA) as indicated were electroporated into E14 neocortices. The percentage of GFP-labeled cells in the VZ, IZ, and CP of E18 neocortical sections was calculated and is plotted as the mean ± s.e.m. (n = 4-5, more than 500 neurons were examined in each condition). **p < 0.01 by two-tailed Welch's *t* test. **(C)** Plasmids expressing a kinase-dead form (D157A) of AMPKα2^{res} (AMPKα2 resistant to AMPKα2 shRNA) and AMPKα2 shRNA were electroporated into E14 neocortices as indicated with the plasmid expressing GFP. The percentage of GFP-positive neurons in the CP, IZ, and VZ of the E18 brain slices was measured and is plotted as the mean ± s.e.m. (n = 4, more than 1000 neurons were examined in each condition). **p < 0.01 by two-tailed Welch's *t* test. NS, not significant. Scale bars, 100 μm.

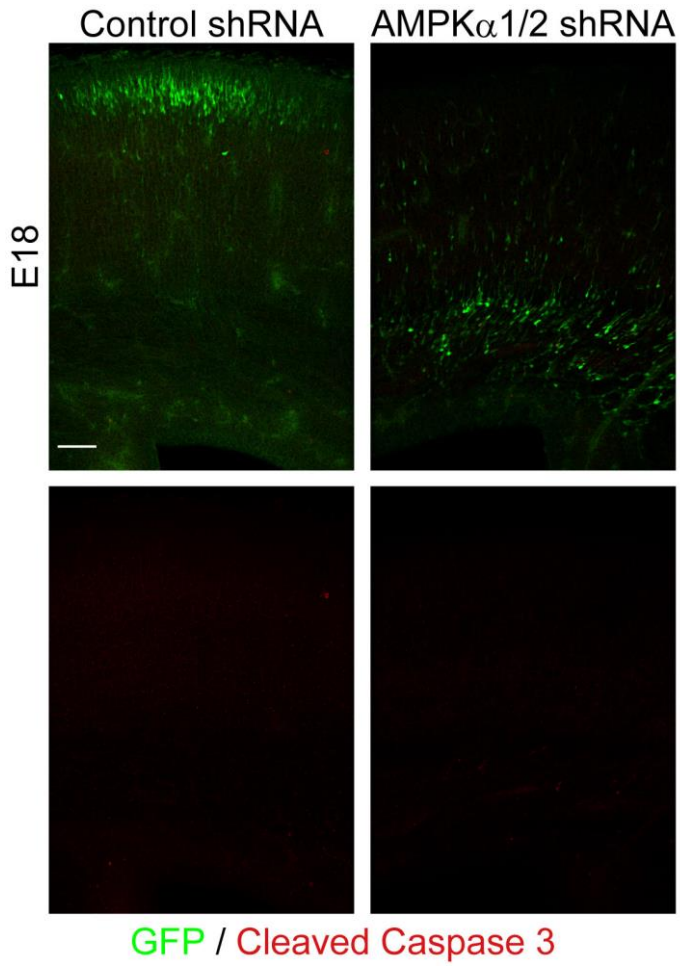

Fig. 10 AMPKα knockdown does not significantly induce apoptosis.

Either the control shRNA plasmid or the AMPKα1/2 shRNA plasmid was electroporated in E14 neocortices together with the GFP-expressing plasmid. E18 brain sections were then immunostained with an antibody against cleaved caspase 3. Nuclei were stained with TO-PRO-3 iodide. Scale bar, 100 μm.

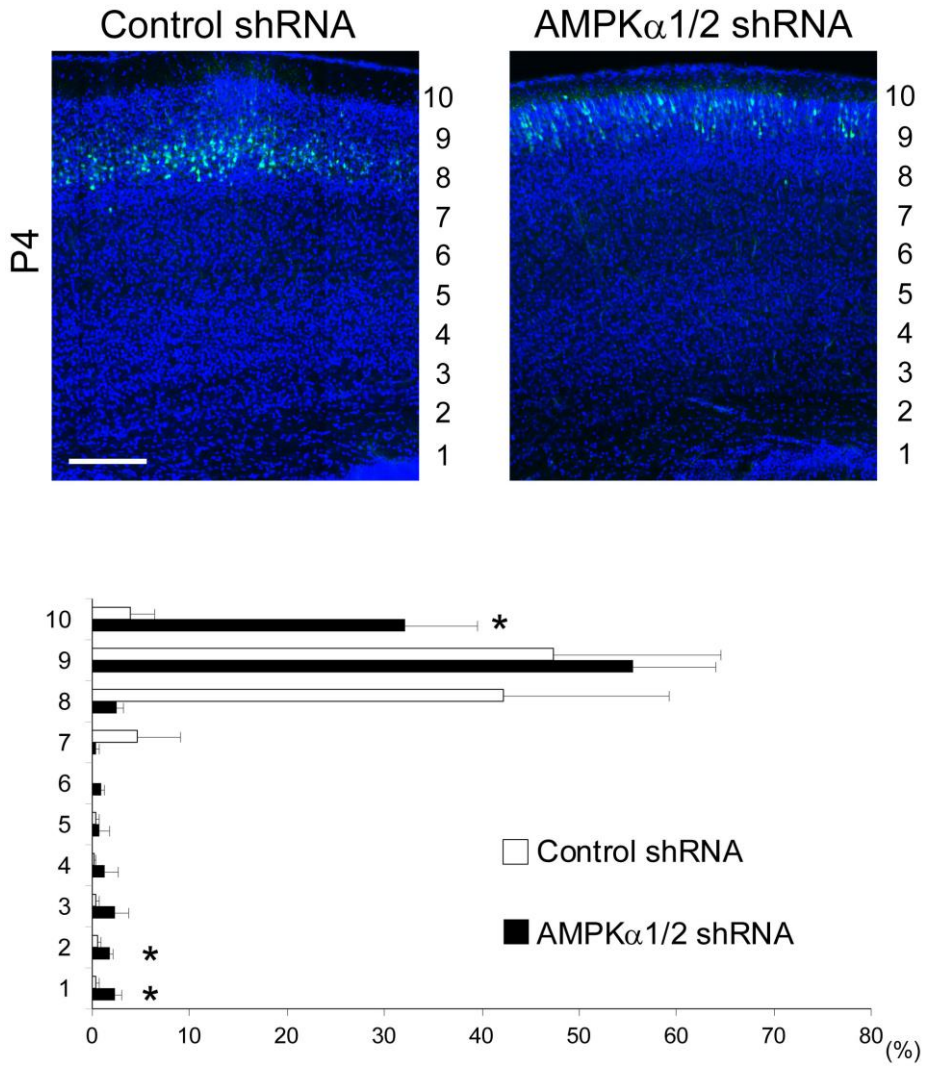

Fig. 11 Delayed migration of AMPKα-depleted neurons.

Either the control shRNA plasmid or the AMPKα1/2 shRNA plasmid was electroporated into E14 neocortices with the plasmid that express GFP. Brain sections were prepared from P4 brains and immunostained with an antibody against GFP. TO-PRO-3 iodide staining shows Nuclei. The positioning of GFP-positive neurons was analyzed by bin analysis. The percentage of GFP-labeled neurons in each bin is plotted as the mean ± s.e.m. (n = 4 embryos, total 749 neurons were analyzed for control shRNA, 522 neurons for AMPKα1/2 shRNA). *$p < 0.05$ versus control shRNA by two-tailed Welch's *t* test. Scale bar, 200 μm.

2-3. AMPKα depletion disrupts nuclear translocation

The directed centrosomal movement and proper nucleus-centrosome coupling are essential for nuclear migration and thus neuronal migration. To investigate the effect of AMPKα knockdown on the positioning of the centrosome and nucleus in migratory neurons, I introduced into E14 embryos the DsRed-Centrin2-expressing plasmid (a maker of the centrosome) and the GFP-expressing plasmid, together with either the control shRNA plasmid or AMPKα1/2 shRNA plasmid. I then analyzed migratory neurons located at upper part of the IZ and lower part of the CP at E17. I found that in AMPKα-depleted neurons, the centrosome was far away from the nucleus (6.13 ± 0.63 μm), when compared with control neurons (1.53 ± 0.33 μm) (Fig. 12A, B). In migrating neurons, the nucleus was often elongated toward the direction of migration, probably due to the application of strong traction forces on the nucleus by dynein (Tsai et al., 2007). The ratio of nuclear length over its width (L/W) of control neurons was 2.42 ± 0.06, while the L/W value of dynein heavy chain-depleted neurons was significantly lower (1.98 ± 0.06) than that of control (Fig. 12A, B). These results support the idea that the distorted nuclear shape is caused by the traction force generated by dynein. Notably, the L/W values of AMPKα-depleted neurons were similar to that of dynein heavy chain-depleted neurons and remarkably lower than control (AMPKα1/2 shRNA, 1.88 ± 0.05; AMPKα1 shRNA, 2.18 ± 0.07; AMPKα2 shRNA, 1.85 ± 0.06) (Fig. 12A, B). These observations indicate that AMPK, just like dynein, is important for spatial positioning of the centrosome/nucleus and proper coordination of the nucleus-centrosome coupling.

To further define the role for AMPKα in migrating neurons, I analyzed the

centrosomal/nuclear behavior in migrating neurons in acute brain slices. For this purpose, I introduced plasmids expressing DsRed-Centrin2, Histone H2B-GFP (nuclear marker) and CFP into neurons, together with either the control shRNA plasmid or the AMPKα1/2 shRNA plasmid. Consistent with previous reports (Tsai et al., 2007; Zhang et al., 2009), control neurons migrated radially in a typical saltatory manner: a cytoplasmic swelling was formed near the base of leading process, the centrosome moved forward at a relatively constant motion until it reached the swelling, and the nucleus moved to the centrosome in a saltatory fashion (Fig. 13A, B). Also, the nucleus appeared distorted toward the direction of migration. On the other hand, AMPKα1/2-depleted neurons showed impaired centrosomal and nuclear movement with the centrosome stuck just ahead of the nucleus or arrested at the swelling formed in the leading process (Fig. 13A, B). In addition, the nucleus of AMPKα1/2-depleted neurons mostly adopted a rounded-shape rather than a distorted shape when compared with control neurons (Fig. 13A). Altogether, these results indicate that AMPK is required for proper nuclear and centrosomal behavior in migratory neurons.

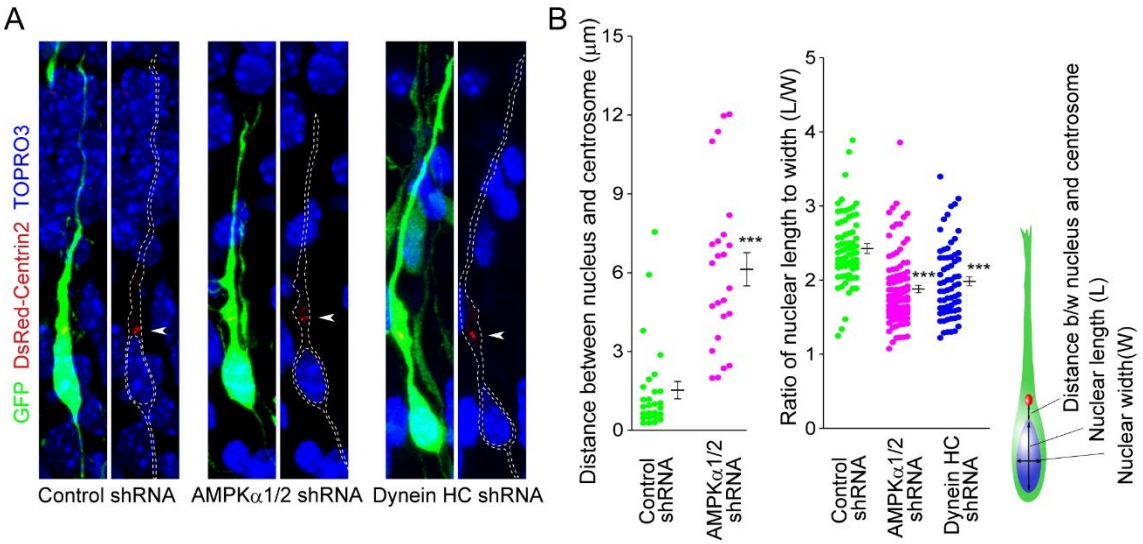

Fig. 12 Knock-down of AMPKα disrupts the nucleus-centrosome coupling.

(A) Plasmids expressing control shRNA, AMPKα1/2 shRNA and dynein heavy chain shRNA (Dynein HC shRNA) were electroporated into E14 neocortices with constructs expressing GFP and DsRed-Centrin2. E17 brain slices were immunostained with anti-GFP antibody. TO-PRO-3 iodide staining shows Nuclei. GFP-labeled migrating neurons in the lower CP and upper IZ were analyzed. Arrowheads show the position of the centrosome labeled by DsRed-Centrin2. The edge of the GFP-positive cells and their nuclei are outlined with dashed lines. **(B)** The distance between the nucleus and the centrosome was measured and is plotted as the mean ± s.e.m. (n = 27 for control shRNA, n = 24 for AMPKα1/2 shRNA) (left). In the right graph, the ratios of the nuclear length over its width (L/W) were measured and are plotted as the mean ± s.e.m. (n = 71 for control shRNA, n = 94 for AMPKα1/2 shRNA, n = 67 for Dynein HC shRNA). ***$p < 0.001$ versus control shRNA by two-tailed Welch's *t* test. Scale bar, 5 μm.

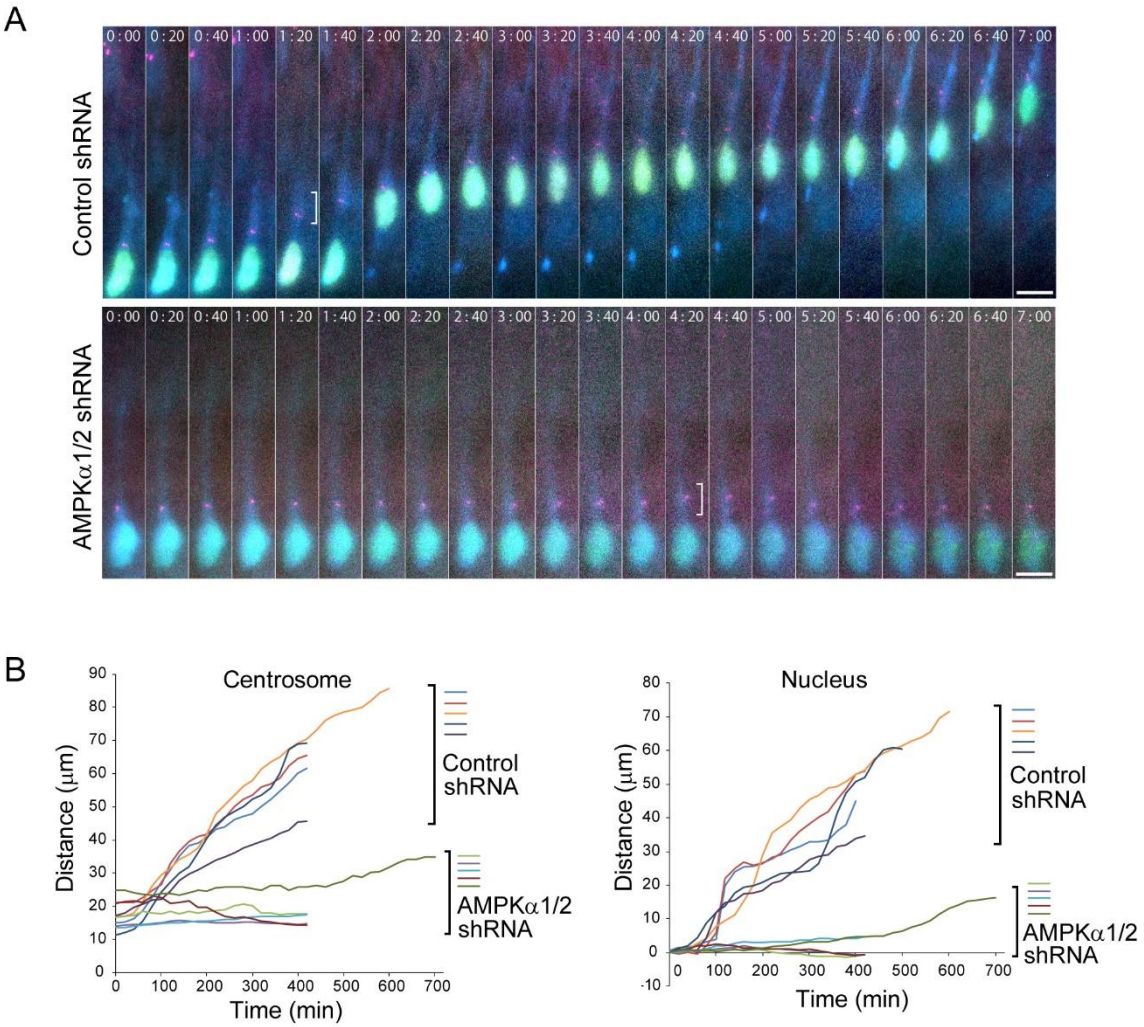

Fig. 13 Knock-down of AMPKα impairs centrosomal and nuclear movement.

(A) Either the control shRNA construct or the AMPKα1/2 shRNA construct was electroporated into E14 cortices with the construct expressing CFP, DsRed-Centrin2-expressing plasmid, and Histone H2B-GFP-expressing plasmid. Coronal brain slices were prepared at E17 and subjected to time-lapse imaging with 20 min intervals over a period of 420-700 min. Time is denoted as hours:minutes in the top of each panel. Brackets indicate the position of the swelling. Scale bars, 10 μm.

(B) Representative tracings of the centrosomal movement and the nuclear movement in control cells and AMPKα1/2-depleted cells are presented in the graph.

2-4. AMPK interacts with cytoplasmic dynein *in vivo*

Given the overlapping distribution of AMPKα with cytoplasmic dynein in cells and the remarkable phenocopy between AMPKα-depleted and dynein heavy chain-depleted neurons, I sought to investigate potential physical interaction of AMPK with cytoplasmic dynein. I first performed co-immunoprecipitation assays using lysates from Cos-7 cells and E17 telencephalon. As shown in Fig. 14A, the dynein intermediate chain (DIC) antibody pulled down DIC as well as the dynein accessory proteins p150glued and Lis1. DIC antibody also co-immunoprecipitated AMPKα as well as pAMPKα (Fig.14A). On the other hand, these proteins are hardly detectable in immunoprecipitates assayed with a control antibody (GFP antibody). Further, Flag-tagged AMPKα and HA-tagged DIC transfected into HEK 293 cells were reciprocally co-immunoprecipitated (Fig. 14B), raising the possibility that AMPKα associates with DIC directly. Together, AMPK physically associates with the cytoplasmic dynein *in vitro* and *in vivo*.

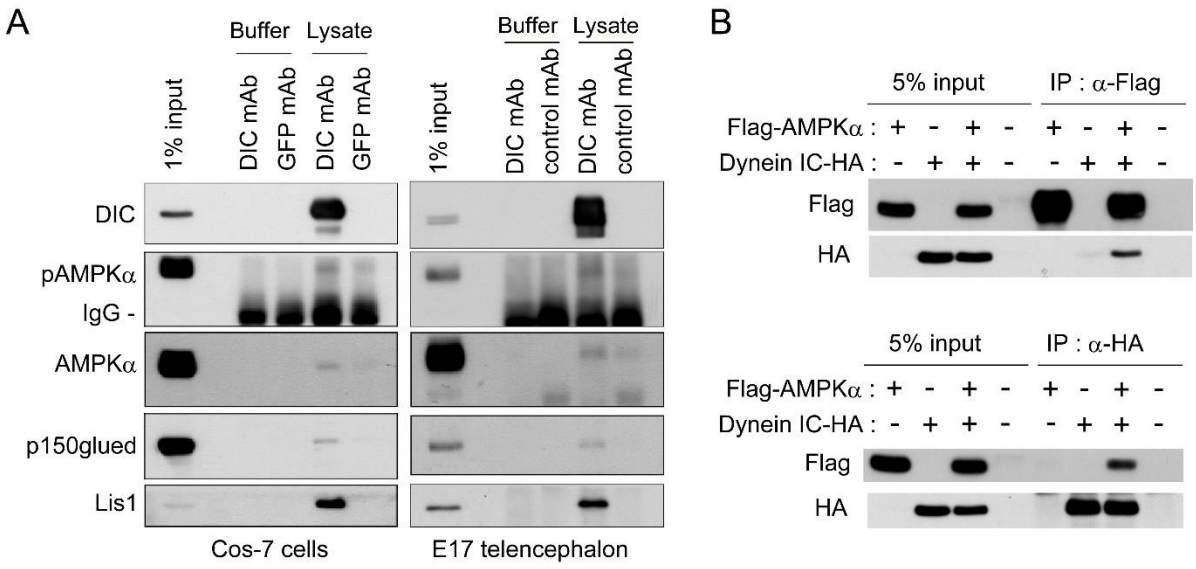

Fig. 14 AMPK interacts with cytoplasmic dynein.

(A) Lysates from E17 telencephalons (right panels) and Cos-7 cells (left panels) as well as control buffer (lysis buffer) were subjected to immunoprecipitation with an anti-DIC antibody (DIC mAb), anti-GFP antibody (GFP mAb) and control IgG (control mAb). Immunoprecipitates were subjected to western blotting with antibodies against pAMPKα, AMPKα, DIC, p150glued and Lis1. Inputs are 1% starting material. **(B)** HEK293 cells were transfected with Flag-tagged AMPKα (Flag-AMPKα) and HA-tagged DIC (Dynein IC-HA) as indicated. Cell lysates were subjected to co-immunoprecipitation with anti-Flag tag antibody (upper panels) and anti-HA tag antibody (lower panels). Immunoprecipitates were immunoblotted with antibodies against Flag-tag and HA-tag. Inputs are 5% starting material.

2-5. AMPK phosphorylates DIC at Ser81

I next tested whether AMPKα interacts with and phosphorylates DIC. For this purpose, phosphate-affinity gel electrophoresis using the acrylamide-pendant Mn^{2+}-Phos-tag (Phos-tag SDS-PAGE)(Kinoshita et al., 2005) was utilized to evaluate the phosphorylation states of DIC. DIC in E13 to P0 neocortical lysates ran as a single band on the normal SDS-PAGE, whereas it ran as two bands on the Phos-tag SDS-PAGE (Fig. 15A). Noticeably, alkaline phosphatase treatment abolished the slower migrating DIC band with a concomitant increase in the faster migrating species (Fig. 15B). These observations suggest that DIC is a phosphoprotein in the developing neocortex and that the slower-migrating DIC corresponds to the phosphorylated species. Similar patterns of phosphorylation state of DIC were also observed in Cos-7 cells and primary cortical neurons (Fig. 15C, D).

When Cos-7 cells were treated with an AMPK activator (A769662), the slower-migrating DIC band intensity increased with a concomitant decrease in the faster-migrating species (Fig. 15E). Conversely, treatment with the AMPK inhibitor Compound C substantially decreased the upper band intensity, and this coincides with an increase in the lower band intensity (Fig. 15E). I also confirmed that AMPK activity increased following treatment with A769662, as which upregulated levels of pAMPKα and of phosphorylated form of acetyl-coenzyme A-carboxylase (ACC), a major AMPK target (Fig. 15E). Conversely, Compound C treatment decreased phosphorylated ACC level (Fig. 15E). Similar results were also obtained in primary neurons treated with AMPK activators (A769662 and AICAR) and an AMPK inhibitor (Compound C) (Fig. 15F). Considering the substantial decrease in the slower-migrating species by treatment

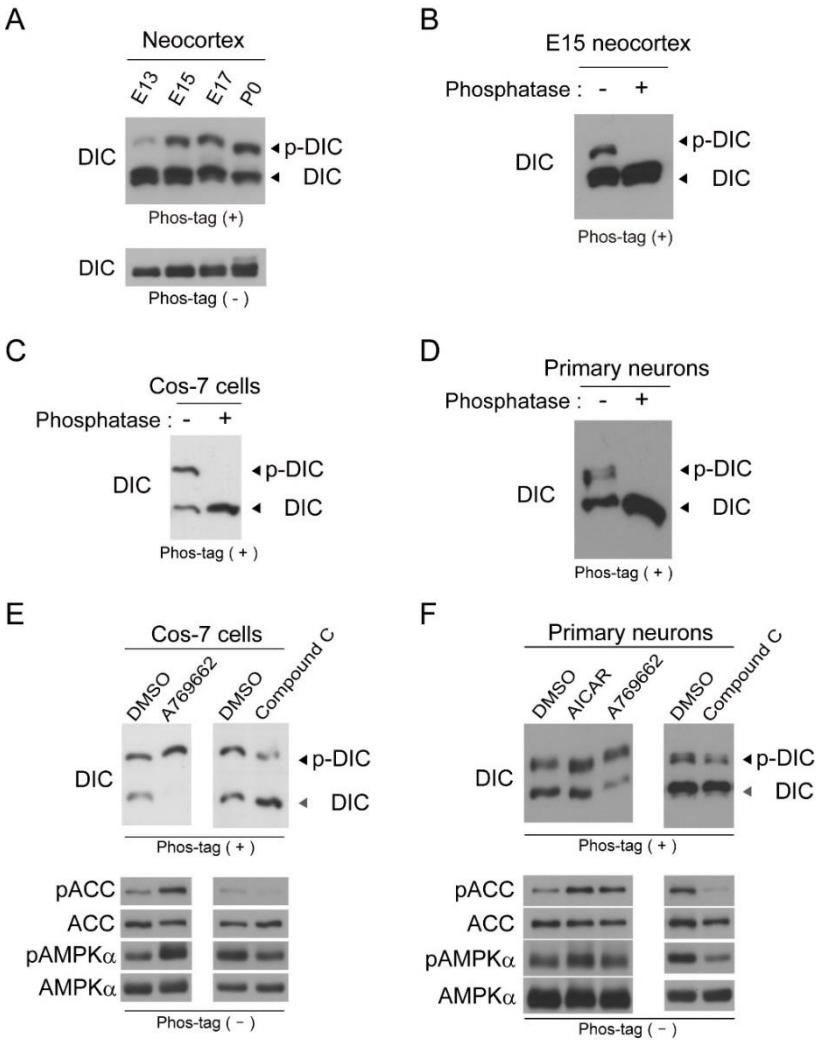

Fig. 15 DIC is a phosphoprotein in the developing neocortex.

(A) Lysates from neocortices (E13, E15, E17 and P0) were subjected to Phos-tag SDS-PAGE (Phos-tag (+), upper panel) and normal SDS-PAGE (Phos-tag (-), lower panel), followed by immunoblotting with a DIC antibody. **(B, C, D)** Lysates from E15 neocortices (B), Cos-7 cells (C) and 4DIV primary neurons (D) were treated with or without alkaline phosphatase and subjected to Phos-tag SDS-PAGE, followed by immunoblotting with a DIC antibody. (**E**, **F**) Cos-7 cells (E) and primary neurons (F) were treated with vehicle (0.2% DMSO), 100 μM A769662 (an AMPK activator), 2 mM AICAR (an AMPK activator) or 20 μM Compound C (an AMPK inhibitor) as indicated for 1 hour. The cell lysates were subjected to Phos-tag SDS-PAGE, followed by immunoblotting with a DIC antibody (upper panels). The lysates subjected to normal SDS-PAGE were also immunoblotted with antibodies indicated (lower panels). Representative results are shown. Similar results were obtained from independent 3-4 experiments.

with Compound C, it is likely that the slower-migrating phospho-species were generated predominantly by endogenous AMPK activity. Consistent with this notion, levels of the slower-migrating species appear to be related to the levels of pAMPKα in the developing neocortex: They are both expressed at low levels at E13 and then are upregulated at E15-P0 (Figs. 4A, 15A). Altogether, these observations indicate that AMPK contributes to phosphorylation of DIC.

To ascertain that AMPKα directly phosphorylates DIC, I performed *in vitro* phosphorylation assay using recombinant proteins. In mammals, there are two different dynein intermediate chain genes, *IC-1* and *IC-2*, and each gene has several splice variants. In our experiments, I used the IC-2B isoform, as it is known to be expressed abundantly in neurons and developing brain (Kuta et al., 2010; Pfister et al., 1996a; Pfister et al., 1996b). I then incubated bacterially expressed, recombinant GST-tagged DIC with recombinant, active AMPKα1/β1/γ2 and thereafter subjected them to normal SDS-PAGE. As shown in Fig. 16A, GST-DIC incubated with active AMPK showed a significant mobility shift. The up-shifted band was detected with an antibody recognizing phospho-Ser (Fig. 16A), suggesting that AMPK directly phosphorylates DIC at Ser residue(s). In order to identify the site(s) of phosphorylation, the up-shifted band of GST-DIC was excised out from the gels and subjected to in-gel tryptic digestion followed by liquid chromatography-tandem mass spectrometry (LC-MS/MS). The mass spectrometry analysis identified two tryptic peptides (42-EAAVSVQEESDLEK-55 and 59-EAEALLQSMGLTTDSPIVPPPMSPSSK-85) each with a single phosphorylation (Fig. 16B). Fragmentation analysis of these peptides revealed the Ser51-phosphorylation in the first peptide and a single phosphorylation between Ser81 and Lys85 of the second peptide. As three Ser residues exist in between, Ser81, Ser83 and

Ser84 in conjunction with Ser51 were considered as the potential phosphorylation sites of DIC by AMPK. Of note, these sites identified are highly conserved among IC-1 and IC-2 splice variants in mammals.

To determine which of these sites is phosphorylated by AMPK, I examined the phosphorylation status of mutant DIC in which each of the four sites was substituted with alanine. I then transfected these mutants (DIC S51A, S81A, S83A, S84A) with the Flag-tag into Cos-7 cells, and cell lysates were subjected to Phos-tag SDS-PAGE followed by western blotting with the Flag antibody. DIC S51A, S83A and S84A mutants retained the slower-migrating species and thus displayed two bands similar to wild-type DIC (Fig. 16C). On the other hand, DIC S81A mutant showed no slower-migrating phospho-species (Fig. 16C). Even in the presence of constitutively active AMPK transfected, the slower-migrating species of DIC S81A were not detected (Fig. 16D). These observations indicate that the substitution of Ser81 is sufficient to block the DIC phosphorylation by AMPK. Similarly, when DIC S81A mutant was introduced into primary cortical neurons, the slower-migrating species were not observed, when compared to neurons transfected with wild-type DIC (Fig. 16E). Thus, Ser81 is the main phosphorylation site for AMPK in neurons.

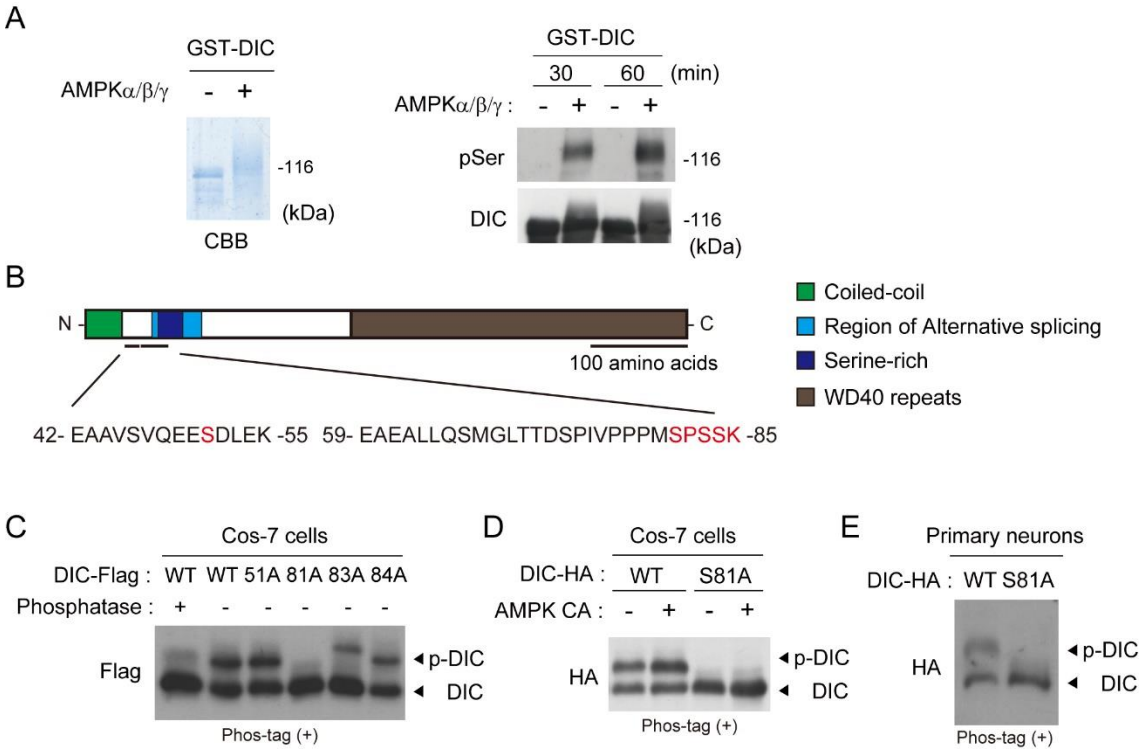

Fig. 16 AMPK phosphorylates DIC at Ser81

(A) Recombinant GST-DIC was incubated with or without recombinant, active AMPKα1/β1/γ2 for 180 min and subjected to SDS-PAGE, followed by Coomassie brilliant blue staining (left panel). The reaction mixtures (incubated for 30 min/60 min) were also subjected to immunoblotting with anti-phospho-Ser antibody (pSer) and anti-DIC antibody (right panels). (**B**) Schematic representation of two tryptic fragments that were identified to be phosphorylated in DIC. Domains present in DIC are also shown. LC-MS/MS fragmentation analysis of GST-DIC incubated with active AMPK identified Ser51-phosphorylation in the first peptide (indicated in red) and a single phosphorylation between Ser81 and Lys85 of the second peptide (indicated in red). **(C)** Lysates from Cos-7 cells transfected with either Flag-tagged wild-type DIC (WT) or Flag-tagged DIC mutants indicated were subjected to Phos-tag SDS-PAGE, followed by immunoblotting with an antibody against Flag-tag. (**D)** Cos-7 cells were transfected with plasmids expressing constitutively active AMPK (AMPK CA), HA-tagged wild-type DIC (WT), HA-tagged DIC S81A as indicated. Cell lysates were subjected to Phos-tag SDS-PAGE, followed by immunoblotting with an antibody against HA-tag. (**E)** Lysates from cultured cortical neurons transfected with either HA-tagged wild-type DIC (WT) or HA-tagged DIC S81A were subjected to Phos-tag SDS-PAGE, followed by immunoblotting with anti-HA antibody.

2-6. AMPK inhibition and forced expression of DIC S81A mutant negatively regulates dynein functions

To determine whether Ser81 phosphorylation of DIC is important for the dynein function, I examined the effect of overexpression of DIC S81A mutant on the dynein-dependent organelle motility. Distribution of the Golgi apparatus is restricted to around the centrosome, and this is maintained by dynein-dependent transport of vesicles towards the minus-ends of microtubules. Indeed, disruption of cytoplasmic dynein activity by knockout of dynein heavy chain or microinjection of a function-blocking DIC antibody causes dispersion of the Golgi apparatus (Burkhardt et al., 1997; Harada et al., 1998). I first analyzed the distribution of the Golgi apparatus in Cos-7 cells transfected with GFP, C-terminally GFP-fused wild-type DIC or C-terminally GFP-fused DIC S81A. In GFP-introduced control cells, the Golgi apparatus, visualized by an antibody against cis-Golgi marker GM130, was clustered at perinuclear region (Fig. 17A). The distribution of the Golgi apparatus in wild-type DIC-introduced cells was indistinguishable from that in control cells (Fig. 17A). In contrast, DIC S81A expression caused significant dispersion of the Golgi apparatus and increased the area marked by GM130 signals (Fig. 17A). Furthermore, similar phenotype (i.e., dispersed distribution of the Golgi apparatus) was observed in Cos-7 cells treated with the AMPK inhibitor Compound C (Fig.17B), suggesting that AMPK activity and Ser81 phosphorylation of DIC positively regulate dynein functions.

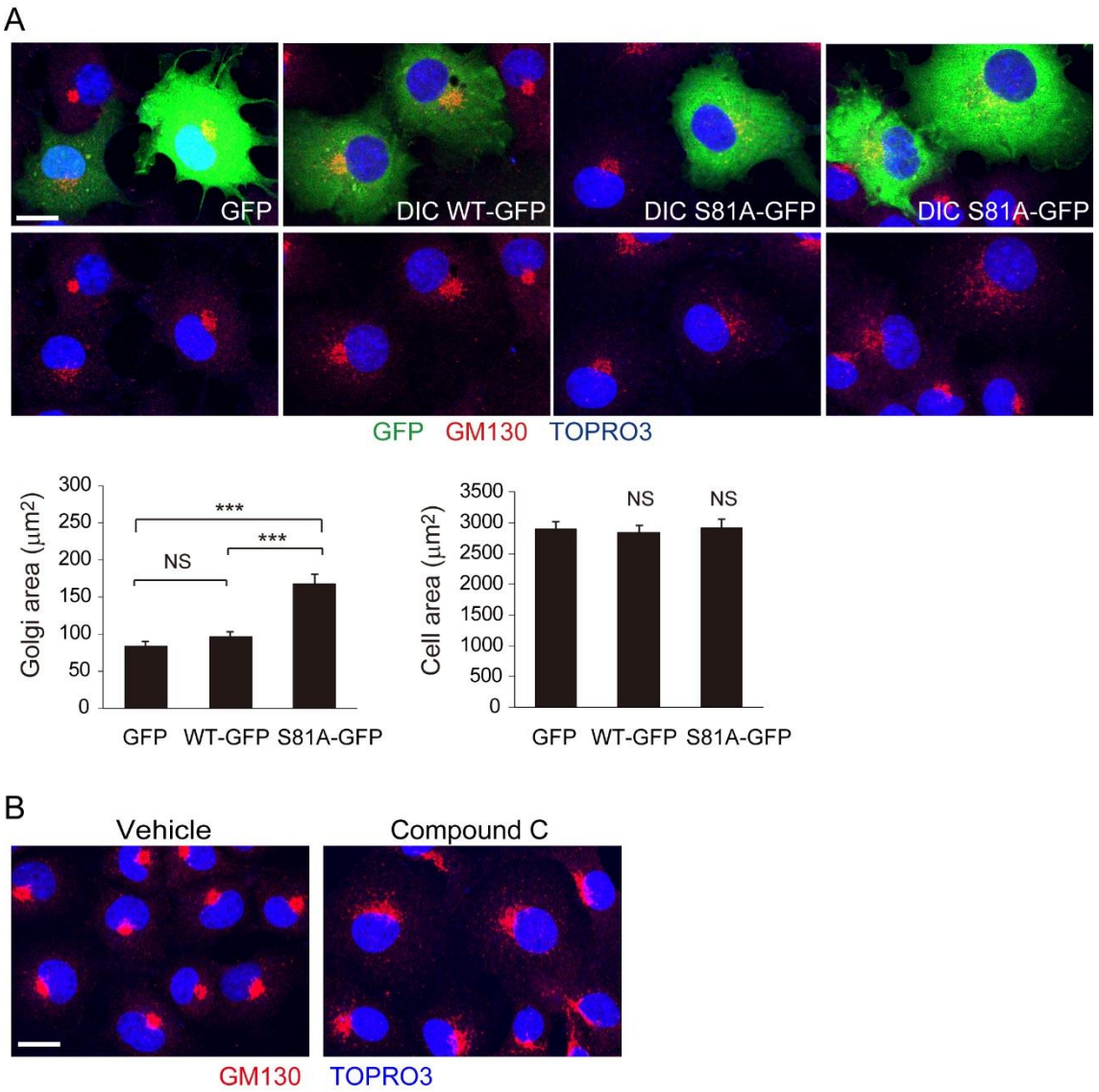

Fig. 17 DIC S81A mutant expression impairs dynein functions

(A) Plasmids expressing GFP, C-terminally GFP-tagged wild-type DIC (DIC WT-GFP) and C-terminally GFP-tagged DIC S81A (DIC S81A-GFP) were transfected into Cos-7 cells as indicated. The cells were fixed 24 hours after transfection and immunostained with anti-GM130 antibody (a cis-Golgi marker). TO-PRO-3 iodide staining shows Nuclei. The Golgi area and cell area of individual transfected cells were measured and are plotted as the mean ± s.e.m. (n = 52 for GFP, n=51 for WT-GFP, n=54 for S81A-GFP). ***p < 0.001 versus control GFP-transfected cells by two-tailed Welch's *t* test. NS, not significant. Scale bar, 10 μm. **(B)** Cos-7 cells were treated with either vehicle (0.2% DMSO) or Compound C (20 μm) for 1 hour and fixed, followed by immunostaining with anti-GM130 antibody. TO-PRO-3 iodide staining shows Nuclei. Scale bar, 10 μm.

2-7. Defects in neuronal migration upon AMPK-depletion are rescued by expression of phospho-mimetic mutant of DIC

I further examined whether Ser81 phosphorylation of DIC contributes to radial migration of cortical neurons. I electroporated plasmids expressing either wild-type DIC or DIC S81A, together with the plasmid expressing GFP, into E14 mouse neocortices and analyzed the distribution of the GFP-labeled neurons at E18. In E18 neocortices electroporated with wild-type DIC, a large fraction of the GFP-labeled neurons was located within the CP (66.3 ± 3.7%), whereas a smaller proportion of the cells was present in the IZ and VZ (Fig. 18A, B). In contrast, in DIC S81A-introduced neocortices the majority of the GFP-labeled cells were located at the IZ (58.6 ± 3.9%), and a small proportion of the cells migrated into the CP (37.8 ± 4.3%) (Fig. 18A, B). Detailed immunohistochemical analysis of migratory neurons electroporated with GFP and DsRed-Centrin2 showed that the nucleus-centrosome distance was remarkably increased in DIC S81A-introduced neurons when compared with control neurons and wild-type DIC-electroporated neurons (control, 2.14 ± 0.35 μm; wild-type DIC, 2.75 ± 0.37 μm, DIC S81A, 5.82 ± 0.64 μm). Also, the L/W ratio of the nucleus in DIC S81A-introduced neurons was significantly lower than those of control and wild-type DIC-introduced neurons (control, 2.51 ± 0.11; wild-type DIC, 2.49 ± 0.08; DIC S81A, 1.87 ± 0.08), but similar to the ratio found in AMPKα-depleted neurons (Fig. 18C, D). These results indicate that overexpression of DIC S81A in neurons disrupts the nucleus-centrosome coupling and impairs neuronal migration, just like AMPKα depletion does.

Finally, I investigated the functional relationship between AMPK and DIC in neuronal migration. I examined the effect of phospho-mimetic mutant of DIC (DIC

S81D) that has Ser81 replaced with Asp to mimic the negative charge generated by phosphorylation. I electroporated the plasmid expressing DIC S81D and control shRNA or AMPKα2 shRNA, into E14 neocortices. The distribution of the GFP-positive neurons in E18 neocortices electroporated with both DIC S81D and control shRNA (Fig. 18E, F) was similar to that of neocortices electroporated solely with control shRNA (Fig. 8A). Thus, DIC S81D expression unlikely affects migration of neurons that have normal levels of AMPKα. Noticeably, mis-positioning of neurons in neocortices electroporated with AMPKα2 shRNA was significantly rescued by overexpression of DIC S81D but was not affected by overexpression of wild-type DIC (Fig. 18E, F). Altogether, AMPK regulates neuronal migration through Ser81 phosphorylation of DIC.

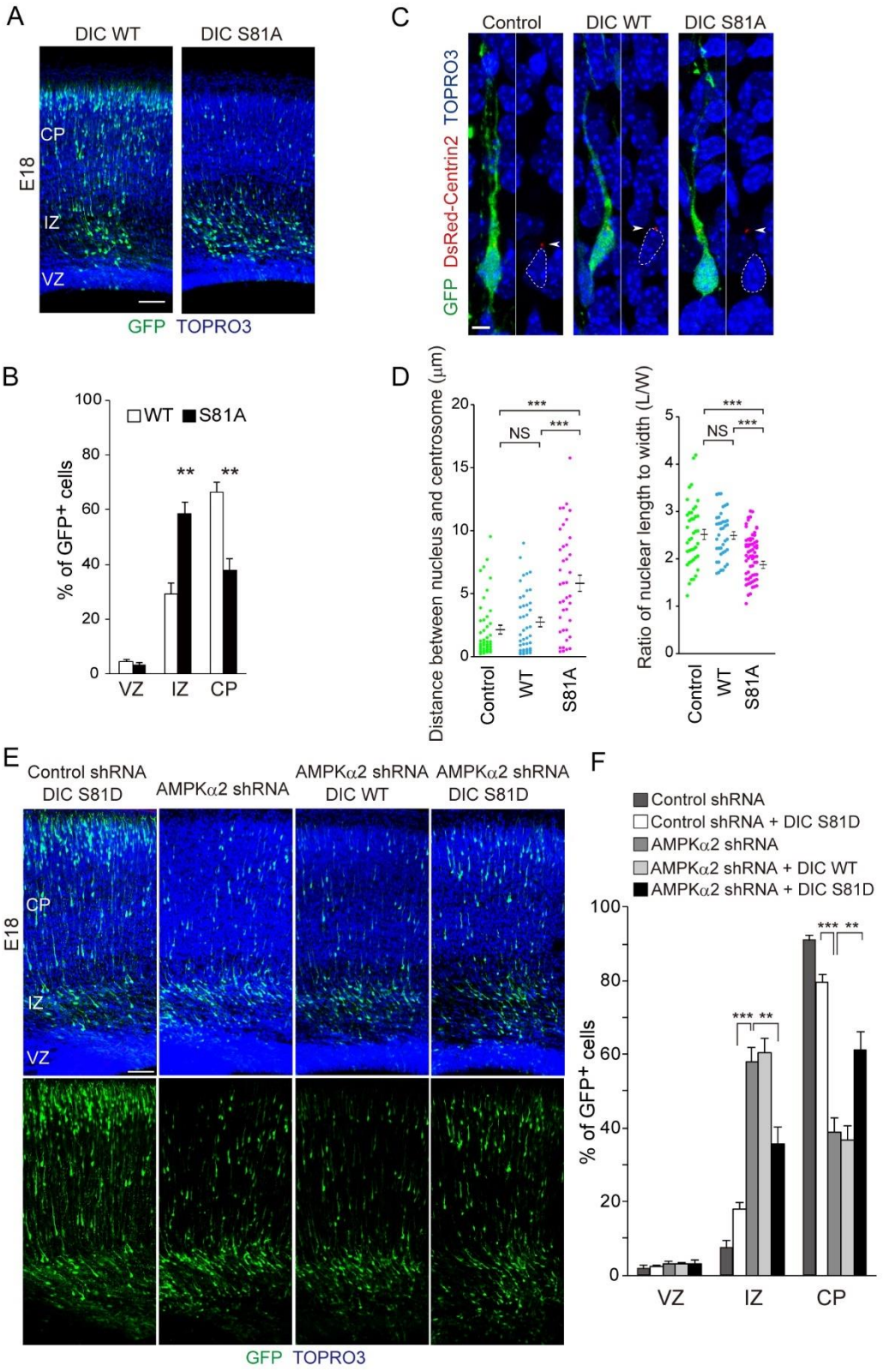
A
DIC WT
DIC S81A
E18
CP
IZ
VZ
GFP TOPRO3
B
WT S81A
% of GFP+ cells
VZ IZ CP
C
Control
DIC WT
DIC S81A
GFP DsRed-Centrin2 TOPRO3
D
Distance between nucleus and centrosome (μm)
Ratio of nuclear length to width (L/W)
NS
Control WT S81A
E
Control shRNA
DIC S81D
AMPKα2 shRNA
AMPKα2 shRNA
DIC WT
AMPKα2 shRNA
DIC S81D
E18
CP
IZ
VZ
GFP TOPRO3
F
Control shRNA
Control shRNA + DIC S81D
AMPKα2 shRNA
AMPKα2 shRNA + DIC WT
AMPKα2 shRNA + DIC S81D
% of GFP+ cells
VZ IZ CP

Fig. 18 Defects in neuronal migration upon AMPK depletion are rescued by expression of phospho-mimetic mutant of DIC.

(A-D) Plasmids expressing wild-type DIC (DIC WT) and DIC S81A were electroporated into E14 neocortices, together with GFP and DsRed-Centrin2, as indicated. E18 brain slices were immunostained with anti-GFP antibody. TO-PRO-3 iodide staining shows Nuclei. (A) Images of the cerebral wall are shown. Scale bar, 100 μm. (B) The percentage of GFP-positive neurons located in the CP, IZ and VZ was measured and is plotted as the mean ± s.e.m. (n = 4 embryos, 1271 neurons were analyzed for DIC WT, 948 neurons for DIC S81A). **p < 0.01 versus wild-type DIC by two-tailed Welch's t test. (C) High magnification images of GFP-labeled migratory neurons are shown. Arrowheads show the position of the centrosome. The nuclei in GFP-positive neurons are outlined with dashed lines. Scale bar, 5 μm. (D) In GFP-labeled neurons at the upper IZ and lower CP, the distance between the nucleus and the centrosome (left graph) and the ratio of the nuclear length over its width (L/W, right graph) were measured and are plotted as the mean ± s.e.m. (n = 44 (control), 42 (DIC WT), 40 (DIC S81A) neurons for the nucleus-centrosome distance, n = 41 (control), 39 (DIC WT), 39 (DIC S81A) neurons for the nuclear shape). ***p < 0.001 by two-tailed Welch's *t* test. NS, not significant. **(E, F)** Plasmids expressing control shRNA, AMPKα2 shRNA, DIC WT and DIC S81D as indicated were electroporated into E14 neocortices with the plasmid expressing GFP. E18 brain slices were immunostained with anti-GFP antibody. TO-PRO-3 iodide staining shows Nuclei. Representative images are shown in (E). Scale bar, 100 μm. (F) The percentage of GFP-labeled cells located in the CP, IZ and VZ was measured and is plotted as the mean ± s.e.m. (n = 4-5 embryos, 1119 neurons were analyzed for control shRNA + DIC S81D, 1014 neurons for AMPKα2 shRNA, 1208 neurons for AMPKα2 shRNA + DIC WT, 1373 neurons for AMPKα2 shRNA + DIC S81D). The data of control shRNA in the graph are derived from Fig. 3B. **p < 0.01, ***p < 0.001 by two-tailed Welch's *t* test.

3. Discussion

AMPK regulates nuclear movement and neuronal migration

Nuclear movement is key for neuronal migration in the developing neocortex. Motor proteins, particularly cytoplasmic dynein, are known to mediate the directed nuclear movement. However, the signals that contribute to dynein's regulation and function during nuclear and neuronal migration remain unclear.

The present study demonstrates that AMPKα is required for proper centrosomal and nuclear migration as well as for neuronal migration in the developing neocortex. I showed that AMPKα depletion causes remarkable retardation of neuronal migration in the developing neocortex (Fig. 8). Importantly, this is associated with disruption of coordination between the centrosome and nucleus, as revealed by the longer centrosome-nucleus distance in the AMPKα-depleted neurons (Fig. 12A, B), and with profound retardation of the centrosomal/nuclear movement, as demonstrated by time-lapse imaging of migratory neurons in brain slices (Fig. 13A, B).

A previous study reported that AMPKα is not required for radial migration in the developing neocortex (Williams et al., 2011). The authors electroporated Cre recombinase with GFP into E15 neocortices of AMPKα1$^{-/-}$; AMPKα2$^{F/F}$ mice to knock out both AMPKα1 and AMPKα2, and, after 5 days culture of dissected brain slices, they analyzed the distribution and morphology of the AMPKα1/α2-deficient cortical neurons. Because approx. 40% of the GFP-labeled neurons were observed into the CP, the authors suggested that AMPK is not required for neuronal migration. There was no statistical analysis for the neuronal distribution but it seems that less GFP-labeled AMPKα1/α2-deficient neurons were present in the CP, and concomitantly more neurons were in the IZ/VZ when compared to the distribution of control GFP-neurons.

The present study shows that AMPKα depletion slows down but does not arrest neuronal migration and that AMPKα-depleted neurons reach the CP by early postnatal stage when AMPKα is knocked down at E14 (6.2% at E17, 28.7% at E18 and >90% at P4)(Figs. 8, 11). Hence, Williams et al. may have not detected migration defects of AMPKα1/α2-deficient cortical neurons due to their experimental time point that is relatively late to detect severe malpositioning.

AMPK-mediated Ser81 phosphorylation of DIC contributes to dynein functions

Cytoplasmic dynein is a large protein complex composed of six subunits (e.g., dynein heavy chain and DIC) that interacts with multiple accessary proteins (e.g., Lis1, Ndel1/Nde1 and p150glued). These accessory molecules and the post-translational modifications of the dynein subunits regulate dynein's functional properties. In this complex, dynein heavy chain forms the motor domain, and DIC has a scaffolding role in the dynein complex. DIC binds to the other four subunits and also associates with several accessary proteins. In cells, Dynein acts as a minus end-directed motor on microtubules and contributes to retrograde transport of its bound organelles/cargoes such as endosomes, Golgi apparatus, mitotic kinetochores, and nuclear envelope (Burkhardt et al., 1997; Echeverri et al., 1996; Harada et al., 1998; Roghi and Allan, 1999; Salina et al., 2002).

As suggested by a proteomics screen for proteins phosphorylated by AMPK in mouse brain extracts, DIC may be a candidate target for AMPK in the brain (Tuerk et al., 2007). In the present study, using lysates from embryonic brain, Cos-7 cells and primary neurons, endogenous and exogenous DIC, phosphatase and AMPK inhibitor treatment, I provided multiple evidences that DIC is phosphorylated by AMPK (Fig.

14). I went on to demonstrate that AMPK directly phosphorylates DIC *in vitro* (Fig. 16) and using recombinant phospho-dead mutants, identified Ser81 as the main site of phosphorylation by AMPK *in vivo* (Fig. 16).

Importantly, I discovered that Ser81 phosphorylation of DIC by AMPK positively regulates dynein functions. Transfection of phospho-resistant DIC S81A mutant into Cos-7 cells leads to disruption of normal perinuclear enrichment of the Golgi apparatus, a measure of dynein function, (Fig. 17). The N-terminal region of DIC contains a coiled-coil domain involved in binding to accessary proteins such as p150glued and Ndel1/Nde1, whereas the C-terminal region is composed of binding sites for other dynein subunits. Ser81 resides in a serine-rich region that is adjacent to the N-terminal coiled-coil domain (see Fig. 16B). Several lines of evidence suggested that dynein functions are modulated by the phosphorylation of DIC at Ser/Thr residues in the serine-rich region. In fact, Ser81 phosphorylation of DIC promotes dynein binding to and dynein-mediated transport of signaling endosomes such as Trk-containing signaling endosomes (Ginty and Segal, 2002; Mitchell et al., 2012). In addition, phosphorylation of Ser88/Thr89 has been shown to cause dissociation of Ndel1, a potent dynein force generator, thereby reducing dynein motility (Gao et al., 2015). Thr89 phosphorylation can also promote dynein binding to the kinetochore protein ZW-10 for dynein localization on kinetochore (Whyte et al., 2008) rather than to p150glued, a mediator for interaction of dynein with various organelles/cargos (Schroer, 2004). Also, live cell imaging of dynein composed of Ser84 phospho-mimetic/phospho-resistant mutants of DIC suggests that phosphorylation at DIC Ser84 modulates dynein motor activity (Blasier et al., 2014). Thus, phosphorylation within the serine-rich domain positively or negatively regulates dynein behaviors through stimulating/inhibiting dynein motor

activity and/or dynein's association with organelles/cargos. In this context, it is hypothesized that Ser81 phosphorylation of DIC promotes dynein motility and/or dynein's association with its targets to promote neuronal migration.

AMPK regulates neuronal migration through Ser81 phosphorylation of DIC

I found that overexpression of phospho-resistant DIC S81A mutant in migratory neurons significantly retards their neuronal migration, just like AMPKα depletion does. Also, overexpression of phospho-mimetic DIC S81D mutant ameliorated migration defects observed upon AMPK depletion. Together with the findings of direct phosphorylation of DIC by AMPK at Ser81 and modulation of dynein behaviors by the Ser81 phosphorylation (see above), I concluded that AMPK contributes to neuronal migration via Ser81-phosphorylation of DIC and positive regulation of dynein functions.

Given that the AMPK-dynein pathway contributes to neuronal migration, it is important to uncover the distribution of AMPK and Dynein in *in vivo* migrating neurons in order to illustrate a model as to where and how these molecules affect nuclear and centrosomal movement. However, immunohistochemical analysis using sections derived from fixed brains is unsuitable for localization analysis, as microtubules become destabilized during the fixation process that is relatively slow and thereby redistribution/diffusion of microtubule-binding protein likely occurs within the cells. Therefore, previous studies have utilized cultured migratory neurons and demonstrated that in migrating neurons the microtubule network emanating from the centrosome extends within the leading process and reward to surround the nucleus. In addition, dynein is enriched at the centrosome, at the nuclear surface and in the swelling near the

base of leading process in migrating neurons (Tsai et al., 2007; Zhang et al., 2009). In the present study, I found that AMPK shows remarkable colocalization with dynein in cultured Cos-7 cells and cultured cortical neurons (Fig. 5), in particular, at the microtubule array and the centrosome. Although in *in vivo* migrating neurons in fixed brain sections, AMPK appears to be enriched predominantly at the centrosome, there is a possibility that microtubule-dependent localization of dynein and AMPK at certain sites (e.g., the nuclear surface and swelling) might be disrupted, due to destabilization of microtubules as mentioned above. Considering the clear colocalization of AMPK and dynein in cultured cells, I speculate that AMPK codistributes with dynein not only at the centrosme but also at the swelling and nuclear surface in *in vivo* migrating neurons.

To date, it has been suggested that dynein attached to the nuclear envelope pulls the nucleus along the microtubules toward the centrosome. In addition, dynein bound to cell membrane at the swelling is thought to pull the microtubules and centrosome toward the swelling, as the swelling appears as an important region where the leading process is attached to the substrate to generate traction forces. This model is supported by the finding that knockdown of dynein HC in migrating neuron causes defect in the centrosomal forward movement, nucleus-centrosome coupling and a rounded-shape of the nucleus rather than a distorted shape (Bellion et al., 2005). In this context, I propose a model in which AMPK that colocalizes/associates with dynein phosphorylates DIC, potentiates dynein functions, and enhances pulling forces on the nucleus and centrosome to direct proper nuclear and centrosomal forward movement (Fig. 19).

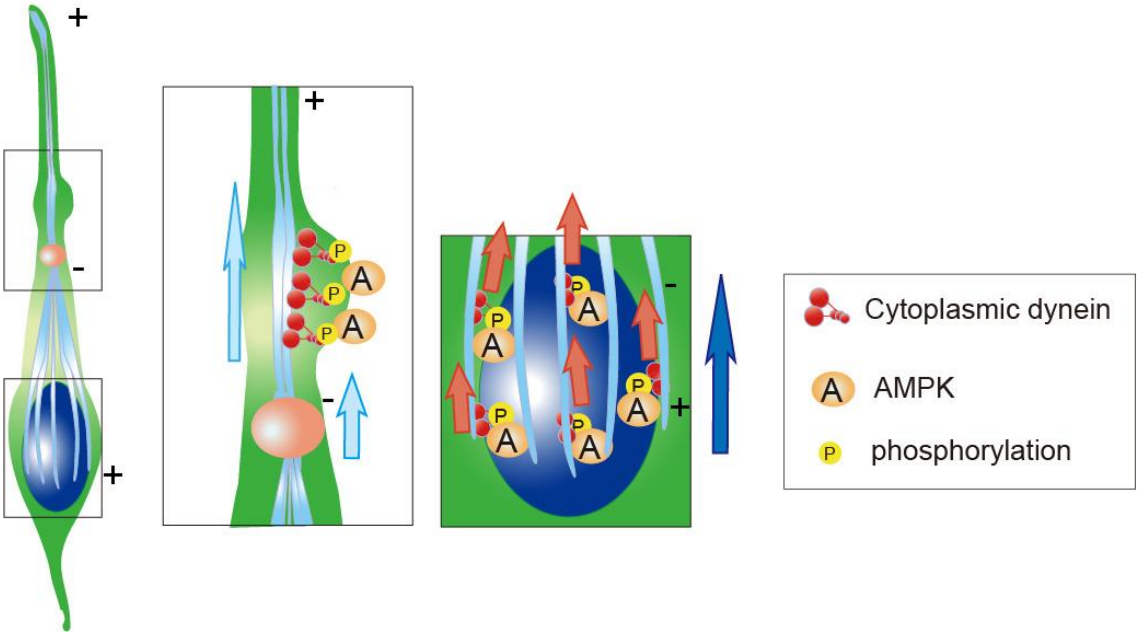

Fig. 19 Model of AMPK-dynein axis function in nuclear and centrosomal forward movement in migrating neurons.

In migrating neurons, dynein at the cell membrane in the swelling of the leading process provides a traction on the microtubule and centrosome (light blue arrows) to direct the centrosomal forward movement (Tsai et al., 2007), and dynein at the nuclear envelope provides traction force on the nucleus (Zhang et al., 2009) toward the centrosome (red arrows) to control nuclear migration (dark blue arrow). AMPK mediates Ser81 phosphorylation of Dynein IC and potentiates the dynein functions probably through modulating dynein motility and/or dynein's association with its targets. Thus, AMPK likely boosts pulling forces on the nucleus and centrosome to direct proper nuclear and centrosomal forward movement in migrating neurons.

4. Conclusion

In this study, I provide novel mechanistic insights into the regulation of dynein function during neuronal migration. I identified AMPK as a regulator for DIC through Ser81 phosphorylation during centrosomal and nuclear movements, both critical for proper neuronal migration. These findings may help understand the molecular basis of neuronal migration disorders.

5. Materials and Methods

Animals

ICR mice were purchased from Japan SLC, Inc. (Hamamatsu, Japan) and were housed under 12-hours light-12 hours dark cycle. All animal experiments were carried out in accordance with guidelines set by The University of Tokyo and approved (permit number 21-01) by the Committee on Animal Care and Use of the Graduate School of Science in The University of Tokyo.

Plasmids

The pCAGEN, pCAG-IRES-GFP (pCAGIG) and pCAG-CFP plasmids were kind gifts from Dr. Takahiko Matsuda (University of Hyogo, Hyogo, Japan). The pBS/U6 plasmid and an RNAi plasmid for dynein heavy chain were kind gifts from Dr. Yang Shi (Harvard Medical School, MA, USA) and Dr. Li-Huei Tsai (Massachusetts Institute of Technology, MA, USA), respectively. The full-length open reading frame (ORF) of *Ampkα1, Ampkα2* and *Dync1I2* were amplified by PCR from cDNA derived from the E16 mouse cortex and cloned into the pCAGEN vector that drives expression of subcloned gene from the CAG promoter. The AMPKα1 and AMPKα2 shRNA plasmids were constructed by insertion of the annealed oligonucleotides into the pBS/U6 plasmid (Sui et al., 2002), as described previously (Sanada and Tsai, 2005). Target sequence for RNAi were as follows: For AMPKα1 shRNA, 5'-GGCACACCCTGGATGAATTAA-3'; For AMPKα1 shRNAi#2, 5'-GGGACTGCTACTCCACAGAGA-3'; AMPKα2 shRNA, 5'- GGTAGACAGTCGGAGCTATCT-3'; For AMPKα2 shRNA#2, 5'-GGATGACAGCGCCATGCATAT -3'. Plasmids encoding silent mutants of AMPKα,

kinase-dead mutants of AMPKα, as well as phospho-resistant and phospho-mimetic mutants of DIC were constructed by the QuickChange mutagenesis technique. Constitutively active mutant of AMPKα2 (C-terminal truncated form of AMPKα2 (amino acids, 1-312), with Thr172 changed to Glu) were generated by the QuickChange mutagenesis followed by subcloning of the 1-312 amino acids region into the pCAGEN vector. pCAG-Histone H2B-GFP plasmids was generated by subcloning histone H2B-GFP from the pBOS-H2BGFP vector (BD Biosciences) into the pCAGEN vector. For bacterial expression, *Dync1I2* was subcloned into the pGEX-4T2 vector that expresses N-terminal GST-tagged Dynein IC2B.

Cell culture and transfection

Cos-7 cells and HEK293 cells were purchased from the European Collection of Authenticated Cell Cultures (ECACC). Cells were maintained in Dulbecco's Modified Eagle Medium (DMEM) supplemented with antibiotics and 10% fetal bovine serum (FBS). Transfection of plasmids into cells were performed using Lipofectamine 2000 (Invitrogen). After transfection, cells were cultured in DMEM with 10% FBS for 24-48 hours prior to being subjected to immunoblotting, immunocytochemistry and immunoprecipitation.

The preparation of primary cortical neurons was performed as described (Asada et al., 2007). Plasmids were transfected into primary neurons by Nucleofector device (Amaxa), according to the manufacturer’s protocols. In some experiments, primary cortical neurons and Cos-7 cells were treated with A769662 (final concentration 100 μM; AdooQ Bioscience), AICAR (2 mM; Wako), Compound C (20 μM; Calbiochem) 1 hour prior to being subjected to immunoblotting and immunocytochemistry.

For immunoblotting and coimmunoprecipitation assay, cultured cortical neurons and Cos-7 cells were lysed with ice-cold lysis buffer (20 mM HEPES, 100 mM NaCl, 1.0% TritonX-100, 2 mM Na_3VO_4, 10 mM NaF, and protease inhibitors (Complete, EDTA-free; Roche); pH 7.4). The cell lysates were incubated 30 min on ice and were centrifuged at 20,000 × g for 10 min. Then, the supernatants were collected as cell extracts.

Immunoblotting

Proteins separated by normal SDS-PAGE and Phos-tag SDS-PAGE were transferred to PVDF membranes (Merck Millipore). Phos-tag SDS-PAGE was performed in typical SDS-PAGE gels (6%) supplemented with 20 μM Phos-tag Acrylamide (Wako; AAL-107) and 80 μM $MnCl_2$. The blots were blocked with 3(w/v)% BSA or 5(w/v)% skim milk in TBS (10 mM Tris-HCl, 140 mM NaCl; pH 7.6) at room temperature for 1 hour, and then incubated with primary antibodies in 3% BSA in TBS overnight at 4°C, and then incubated with secondary antibodies at 4°C overnight.

Primary antibodies used were as follows. Rabbit anti-AMPKα (1:1000; #2532, Cell Signaling Technology), rabbit anti-pT172-AMPKα [40H9] (1:1000; #2535, Cell Signaling Technology), rabbit anti-AMPKα1 [Y365] (1:1000; ab32047, Abcam), rabbit anti-AMPKα2(1:1000; ab3760, Abcam), rabbit anti-phospho-ACC (Ser79) [D7D11] (1:1000; #4150, Cell Signaling Technology), rabbit anti-ACC [C83B10] (1:1000; #3676, Cell Signaling Technology), mouse anti-Dynein IC [74.1] (1:3000; sc-13524, Santa Cruz Biotechnology), rabbit anti-Dynein HC (1:1000; R-325, sc-9115, Santa Cruz Biotechnology), mouse anti-p150glued (1:2000; 610473, BD Biosciences), goat anti-LIS1 (1:200; N-19, sc-7577, Santa Cruz Biotechnology), rabbit anti-phosphoserine

(1:1000; 61-8100, Invitrogen), mouse anti-DYKDDDDK (1:10000; 014-22383, Wako), mouse anti-Flag (1:1000; F1804, Sigma), rabbit anti-HA (1:2000; 561, MBL) , rabbit anti-GFP (1:1000; A11122, Invitrogen), and mouse anti-β-actin (1:20000; A1978, Sigma). The secondary antibodies used were HRP (horseradish peroxidase)-conjugated anti-mouse IgG antibody (GE Healthcare), HRP-conjugated anti-rabbit IgG antibody (GE Healthcare) and HRP-conjugated anti-goat IgG antibody (Kirkegaard and Perry Laboratories).

Coimmunoprecipitation assay

E17 telencephalons (4 hemispheres) isolated were incubated in HBSS containing DNase I and trypsin at 37°C for 20 min, and triturated with a fire-polished Pasteur pipet, followed by rinsing with HBSS three times. The telencephalic cells were lysed with the lysis buffer as above.

Cell extracts from E17 telencephalon and Cos-7 cells were precleared by incubation with 20 μl of Protein G-Sepharose for 30 min at 4°C, and then incubated with anti-Dynein IC antibody [74.1] (5 μg), or mouse anti-GFP antibody (5 μg), or control IgG (5 μg; Sigma) at 4°C for 24 hours, and thereafter incubated with 20 μl of Protein G-Sepharose for 1 hour. The Protein G-Sepharose beads were washed three times with lysis buffer and subjected to western blotting.

Lysates of HEK293 cells transfected with or without plasmids expressing Flag-AMPKα2 and Dynein IC-HA were prepared 48 hours after transfection of plasmids. Then, the cells lysates were subjected to coimmunoprecipitation assay with anti-Flag antibody (2 μg) or anti-HA antibody (2 μg).

Immunocytochemistry

For immunostaining, cells were fixed in 4% paraformaldehyde/PBS at 37°C for 15 min, permeabilized with 0.1% Triton X-100/PBS for 5 min and blocked with PBS containing 0.2% Triton X-100 and 3% BSA. The cells were incubated with primary antibodies at 4°C overnight, followed by incubation with Cy3/Cy5/Alexa 488-conjugated secondary antibodies. For immunostaining with anti-Dynein IC [74.1] antibody, cells were fixed with methanol at -20°C for 10 min and were subjected to immunostaining as above. For measurements of the size of the Golgi apparatus, the outer edge of the region where GM130 signals are clustered was outlined. Also, the outer edge of cells was outlined based on the GFP image. Then the outlined area size was calculated using ZEN software (Carl Zeiss Microimaging).

Primary antibodies used were as follows. Rabbit anti-AMPKα (1:100; #2532, Cell Signaling Technology), rabbit anti-pT172-AMPKα [40H9] (1:100; #2535, Cell Signaling Technology), mouse anti-Dynein IC [74.1] (1:50; sc-13524, Santa Cruz Biotechnology), goat anti-LIS1 (1:200; N-19, sc-7577, Santa Cruz Biotechnology), rat anti-GFP (1:1000; 04434-34, Nacalai Tesque), mouse anti-Pericentrin (1:200; 611814, BD Biosciences), mouse anti γ-tubulin [GTU-88] (1:200; T6557, Sigma), mouse anti-Tuj1 antibody (1:3000; MMS-435P, Covance) , mouse anti-GM130 (1:100; 610822, BD Biosciences), and mouse anti-α-tubulin (1:1000; T5168, Sigma).

***In utero* electroporation**

DNA solution (approx. 1 μl) in PBS containing 0.01% fast green was injected into the lateral ventricle of mouse embryos, followed by electroporation. The electric pulses

were generated by CUY21-EDIT (Nepa gene) and applied to the cerebral wall at five repeats of 42 V for 50 msec with an interval of 950 msec with forceps-type electrodes (CUY650P5, Nepa gene). The GFP-expressing plasmid was co-injected with the shRNA construct at a concentration ratio of 2:5. Final concentrations of the plasmids used were, AMPKα shRNAs (2-5 μg/μl), DsRed-Centrin2 (5 μg/μl), AMPKα1/AMPKα2 with a silent mutation (5 μg/μl), kinase-dead AMPKα (5 μg/μl) and wild-type/mutant DIC (2-10 μg/μl).

For time-lapse imaging of migratory neurons, the CFP-expressing plasmid (2.5 μg/μl, pCAG-CFP), Histone H2B-GFP expressing plasmid (1 μg/μl), DsRed-Centrin2-expressing plasmid (5 μg/μl) were co-injected with the shRNA constructs (5 μg/μl).

Immunohistochemistry

Brains were dissected and fixed in 4% paraformaldehyde in PBS at 4°C overnight. Vibratome sections (30 μm thickness for immunohistochemistry with anti-pAMPKα antibody, 60 μm for the others) from fixed brains were blocked with PBS containing 0.2% Triton X-100 and 3% BSA, and then subjected to immunohistochemistry as described (Asada and Sanada, 2010).

Primary antibodies used were rabbit anti-AMPKα (1:50; #2532, Cell Signaling Technology), rabbit anti-pT172-AMPKα [40H9] (1:50; #2535, Cell Signaling Technology), rabbit anti-GFP (1:1000; A11122, Invitrogen), rat anti-GFP (1:1000; 04434-34, Nacalai Tesque), rabbit anti-HA (1:1000; #3724, Cell Signaling Technology), and mouse anti-Pericentrin (1:200; 611814, BD Biosciences), rabbit anti-cleaved caspase 3 (1:500, #9661, Cell Signaling Technology).

Time-lapse imaging of acute brain slices

Acute brain slices of mouse embryos were prepared as described (Sanada and Tsai, 2005; Asada and Sanada, 2010) with a few modifications. Mouse embryos were electroporated at E14 and brains were dissected at E17 in ice-cold dissection media (DMEM/F12 supplemented with D-glucose (final concentration, 6.05 g/L)) that was oxygenized and conditioned with 95% O_2/5% CO_2 for 20 min on ice. Vibratome slices (300 μm thickness) were prepared in the ice-cold and preconditioned dissection media. The brain slices were transferred onto glass bottom dishes (Matsunami Glass), and were coated with collagen (Cellmatrix Type I-A, Nitta Gelatin), and placed in a CO_2 incubator for 10 min for the solidification of the collagen. Then, 1 ml of prewarmed culture media (Neurobasal medium supplemented with 5% FBS, 5% horse serum and B-27 supplement) was added into the dish, and brain slices were incubated in a CO_2 incubator for 1hour before observation.

Migrating neurons labeled with fluorescent proteins were observed under 5% CO_2/95% air at 37°C in a PM S1 incubator using the Axio Observer inverted microscope (Carl Zeiss Microimaging). Time-lapse images were obtained with an AxioCam cooled CCD camera (Carl Zeiss Microimaging) every 20 min for 7-12 hours.

Protein kinase assay

Bacterially expressed GST-Dynein IC2B was purified using a glutathione-Sepharose column (GE Healthcare) according to the manufacturer's instructions. Recombinant GST-Dynein IC2B analyzed by SDS-PAGE with Coomassie brilliant blue staining, and protein content was estimated by densitometry of band intensities in the SDS-PAGE gel

compared to those of serially diluted BSA standards. Active AMPK complex (AMPK α1/β1/γ2) were purchased from Signalchem (#P55-10H). Recombinant bacterially-expressed GST-Dynein IC2B (300 ng) was incubated with or without 100 ng of the recombinant AMPK in 20 μl of kinase reaction buffer (20 mM Hepes, 10 mM $MgCl_2$, 1 mM DTT, 1 mM ATP, 0.2 mM AMP, pH7.4) for indicated time at 30°C. The reaction was started by addition of ATP solution and stopped by SDS-PAGE loading buffer.

Mass spectrometry analysis

Recombinant bacterially-expressed GST-DIC (3 μg) was phosphorylated with 1 μg of recombinant active AMPK *in vitro* (see above) followed by subjecting to SDS-PAGE. The GST-DIC band was excised out from the gel and was subjected to in-gel digestion with modified trypsin (sequencing grade, Promega). Mass spectrometry (MS) analysis of digested peptides was carried out by Genomine, Inc. In brief, the tryptic peptides extracted from the gel were separated and analyzed by reversed phase capillary HPLC (high performance liquid chromatography) tandem mass spectrometry (Finnnigan LCQ). The respective spectra from MS/MS were processed using the TurboSEQUEST (Thermo Scientific, San Jose, CA). The generated peak list files were utilized to query NCBI or MSDB database using the MASCOT software. Significant hits as defined by MASCOT probability analysis were taken into account.

Statistical analysis

All bar graphs were plotted as mean ± s.e.m.. Direct comparisons were made using two-tailed Welch's *t* test using Microsoft Excel. The significance level was set at $p < 0.05$. Sample sizes used in the present study are similar to those generally employed in the

field. The experiments were randomized, and collection and analyses of data were performed under blinded experimental conditions.

6. References

Asada, N. and Sanada, K. (2010). LKB1-Mediated Spatial Control of GSK3 and Adenomatous Polyposis Coli Contributes to Centrosomal Forward Movement and Neuronal Migration in the Developing Neocortex. *J. Neurosci.* **30**, 8852–8865.

Asada, N., Sanada, K. and Fukada, Y. (2007). LKB1 Regulates Neuronal Migration and Neuronal Differentiation in the Developing Neocortex through Centrosomal Positioning. *J. Neurosci.* **27**, 11769–11775.

Bellion, A., Baudoin, J. P., Alvarez, C., Bornens, M. and Métin, C. (2005). Nucleokinesis in tangentially migrating neurons comprises two alternating phases: Forward migration of the Golgi/centrosome associated with centrosome splitting and myosin contraction at the rear. *J. Neurosci.* **25**, 5691–5699.

Bertipaglia, C., Gonçalves, J. C. and Vallee, R. B. (2018). Nuclear migration in mammalian brain development. *Semin. Cell Dev. Biol.* **82**, 57–66.

Blasier, K. R., Humsi, M. K., Ha, J., Ross, M. W., Smiley, W. R., Inamdar, N. A., Mitchell, D. J., Lo, K. W. H. and Pfister, K. K. (2014). Live cell imaging reveals differential modifications to cytoplasmic dynein properties by phospho- and dephosphomimic mutations of the intermediate chain 2C S84. *J. Neurosci. Res.* **92**, 1143–1154.

Burkhardt, J. K., Echeverri, C. J., Nilsson, T. and Vallee, R. B. (1997). Overexpression of the dynamitin (p50) subunit of the dynactin complex disrupts dynein-dependent maintenance of membrane organelle distribution. *J. Cell Biol.* **139**, 469–484.

Cooper, J. A. (2013). Mechanisms of cell migration in the nervous system. *J. Cell Biol.* **202**, 725–734.

Dasgupta, B. and Chhipa, R. R. (2016). Evolving Lessons on the Complex Role of AMPK in Normal Physiology and Cancer. *Trends Pharmacol. Sci.* **37**, 192–206.

Echeverri, C. J., Paschal, B. M., Vaughan, K. T. and Vallee, R. B. (1996). Molecular characterization of the 50-kD subunit of dynactin reveals function for the complex in chromosome alignment and spindle organization during mitosis. *J. Cell Biol.* **132**, 617–633.

Feng, Y. and Walsh, C. A. (2001). Protein–Protein interactions, cytoskeletal regulation and neuronal migration . *Nat. Rev. Neurosci.* **2**, 408–416.

Gao, F. J., Hebbar, S., Gao, X. A., Alexander, M., Pandey, J. P., Walla, M. D., Cotham, W. E., King, S. J. and Smith, D. S. (2015). GSK-3β Phosphorylation of Cytoplasmic Dynein Reduces Ndel1 Binding to Intermediate Chains and Alters Dynein Motility. *Traffic* **16**, 941–961.

Ginty, D. D. and Segal, R. A. (2002). Retrograde neurotrophin signaling: Trk-ing along the axon. *Curr. Opin. Neurobiol.* **12**, 268–274.

Guerrini, R. and Parrini, E. (2010). Neuronal migration disorders. *Neurobiol. Dis.* **38**, 154–166.

Harada, A., Takei, Y., Kanai, Y., Tanaka, Y., Nonaka, S. and Hirokawa, N. (1998). Golgi vesiculation and lysosome dispersion in cells lacking cytoplasmic dynein. *J. Cell Biol.* **141**, 51–59.

Hatten, M. E. (1999). CENTRAL NERVOUS SYSTEM NEURONAL MIGRATION. *Annu. Rev. Neurosci.* **22**, 511–539.

Jaleel, M., McBride, A., Lizcano, J. M., Deak, M., Toth, R., Morrice, N. A. and Alessi, D. R. (2005). Identification of the sucrose non-fermenting related kinase SNRK, as a novel LKB1 substrate. *FEBS Lett.* **579**, 1417–1423.

Jeon, S.-M. (2016). Regulation and function of AMPK in physiology and diseases. *Exp. Mol. Med.* **48**, e245–e245.

Kato, M. and Dobyns, W. B. (2003). Lissencephaly and the molecular basis of neuronal migration. *Hum. Mol. Genet.* **12**, R89–R96.

Kinoshita, E., Kinoshita-Kikuta, E., Takiyama, K. and Koike, T. (2005). Phosphate-binding Tag, a New Tool to Visualize Phosphorylated Proteins. *Mol. Cell. Proteomics* **5**, 749–757.

Kriegstein, A. R. and Noctor, S. C. (2004). Patterns of neuronal migration in the embryonic cortex. *Trends Neurosci.* **27**, 392–399.

Kuta, A., Deng, W., Morsi El-Kadi, A., Banks, G. T., Hafezparast, M., Pfister, K. K. and Fisher, E. M. C. (2010). Mouse Cytoplasmic Dynein Intermediate Chains: Identification of New Isoforms, Alternative Splicing and Tissue Distribution of Transcripts. *PLoS One* **5**, e11682.

Lizcano, J. M., Göransson, O., Toth, R., Deak, M., Morrice, N. A., Boudeau, J., Hawley, S. A., Udd, L., Mäkelä, T. P., Hardie, D. G., et al. (2004). LKB1 is a master kinase that activates 13 kinases of the AMPK subfamily, including MARK/PAR-1. *EMBO J.* **23**, 833–843.

Marín, O., Valiente, M., Ge, X. and Tsai, L. H. (2010). Guiding neuronal cell migrations. *Cold Spring Harb. Perspect. Biol.* **2**, 1–21.

Mitchell, D. J., Blasier, K. R., Jeffery, E. D., Ross, M. W., Pullikuth, A. K., Suo, D., Park, J., Smiley, W. R., Lo, K. W.-H., Shabanowitz, J., et al. (2012). Trk Activation of the ERK1/2 Kinase Pathway Stimulates Intermediate Chain Phosphorylation and Recruits Cytoplasmic Dynein to Signaling Endosomes for Retrograde Axonal Transport. *J. Neurosci.* **32**, 15495–15510.

Pfister, K. K., Salata, M. W., Dillman, J. F., Torre, E. and Lye, R. J. (1996a). Identification and developmental regulation of a neuron-specific subunit of cytoplasmic dynein. *Mol. Biol. Cell* **7**, 331–43.

Pfister, K. K., Salata, M. W., Dillman, J. F., Vaughan, K. T., Vallee, R. B., Torre, E. and Lye, R. J. (1996b). Differential expression and phosphorylation of the 74-kDa intermediate chains of cytoplasmic dynein in cultured neurons and glia. *J. Biol. Chem.* **271**, 1687–1694.

Reiner, O., Karzbrun, E., Kshirsagar, A. and Kaibuchi, K. (2016). Regulation of neuronal migration, an emerging topic in autism spectrum disorders. *J. Neurochem.* **136**, 440–456.

Roghi, C. and Allan, V. J. (1999). Dynamic association of cytoplasmic dynein heavy chain 1a with the Golgi apparatus and intermediate compartment. *J. Cell Sci.* **112**, 4673 LP – 4685.

Salina, D., Bodoor, K., Eckley, D. M., Schroer, T. A., Rattner, J. B. and Burke, B. (2002). Cytoplasmic dynein as a facilitator of nuclear envelope breakdown. *Cell* **108**, 97–107.

Schaar, B. T. and McConnell, S. K. (2005). Cytoskeletal coordination during neuronal migration. *Proc. Natl. Acad. Sci. U. S. A.* **102**, 13652–13657.

Schroer, T. A. (2004). DYNACTIN. *Annu. Rev. Cell Dev. Biol.* **20**, 759–779.

Shu, T., Ayala, R., Nguyen, M. D., Xie, Z., Gleeson, J. G. and Tsai, L. H. (2004). Ndel1 operates in a common pathway with LIS1 and cytoplasmic dynein to regulate cortical neuronal positioning. *Neuron* **44**, 263–277.

Solecki, D. J., Trivedi, N., Govek, E. E., Kerekes, R. A., Gleason, S. S. and Hatten, M. E. (2009). Myosin II motors and F-actin dynamics drive the coordinated

movement of the centrosome and soma during CNS glial-guided neuronal migration. *Neuron* **63**, 63–80.

Stein, S. C., Woods, A., Jones, N. A., Davison, M. D. and Carling, D. (2000). The regulation of AMP-activated protein kinase by phosphorylation. *Biochem. J.* **345 Pt 3**, 437–443.

Tanaka, T., Serneo, F. F., Higgins, C., Gambello, M. J., Wynshaw-Boris, A. and Gleeson, J. G. (2004). Lis1 and doublecortin function with dynein to mediate coupling of the nucleus to the centrosome in neuronal migration. *J. Cell Biol.* **165**, 709–721.

Tsai, L. H. and Gleeson, J. G. (2005). Nucleokinesis in neuronal migration. *Neuron* **46**, 383–388.

Tsai, J. W., Bremner, K. H. and Vallee, R. B. (2007). Dual subcellular roles for LIS1 and dynein in radial neuronal migration in live brain tissue. *Nat. Neurosci.* **10**, 970–979.

Tuerk, R. D., Thali, R. F., Auchli, Y., Rechsteiner, H., Brunisholz, R. A., Schlattner, U., Wallimann, T. and Neumann, D. (2007). New Candidate Targets of AMP-Activated Protein Kinase in Murine Brain Revealed by a Novel Multidimensional Substrate-Screen for Protein Kinases. *J. Proteome Res.* **6**, 3266–3277.

Whyte, J., Bader, J. R., Tauhata, S. B. F., Raycroft, M., Hornick, J., Pfister, K. K., Lane, W. S., Chan, G. K., Hinchcliffe, E. H., Vaughan, P. S., et al. (2008). Phosphorylation regulates targeting of cytoplasmic dynein to kinetochores during mitosis. *J. Cell Biol.* **183**, 819–834.

Williams, T., Courchet, J., Viollet, B., Brenman, J. E. and Polleux, F. (2011). AMP-

activated protein kinase (AMPK) activity is not required for neuronal development but regulates axogenesis during metabolic stress. *Proc. Natl. Acad. Sci.* **108**, 5849–5854.

Zhang, X., Lei, K., Yuan, X., Wu, X., Zhuang, Y., Xu, T., Xu, R. and Han, M. (2009). SUN1/2 and Syne/Nesprin-1/2 Complexes Connect Centrosome to the Nucleus during Neurogenesis and Neuronal Migration in Mice. *Neuron* **64**, 173–187.

7. Acknowledgements

I would like to show my greatest appreciation to my supervisor, Professor Yoshikado Sanada, for his valuable discussion and advice. I would like to appreciate Dr. Naoyuki Asada for his helpful comments and advice for experimental techniques. I am grateful to Dr. Minh Dang Nguyen for his advice, to Dr. Takahiko Matsuda for providing pCAGEN, pCAGIG, pCAG-CFP plasmids, to Dr. Li-Huei Tsai for providing the Dynein HC shRNA plasmid, to Dr. Yang Shi for providing the pBS-U6 plasmid. I would like to thank Dr. Nobuhiro Kurabayashi and the other members of Sanada laboratory for their valuable suggestions and discussion.